DOI: 10.26599/FSHW.2026.9251132

Contents lists available at SciOpen

Food Science and Human Wellness

journal homepage: https://www.sciopen.com/journal/2097-0765

China Food Publishing Co.

Design of Maize Starch-Based Pickering Emulsions: Effects on Lipid Digestion, Absorption, and Duodenal Transcriptomics

Nan Zhang[#1,2], Chao Zhang[#1], Yu Zhang[1], Xia Liu[1], Xueyan Gao[3], Yonghao Li[3], Xuan Hu[1,4], Wei Liu*[1], Lingfei Li[2*].

[1] *Institute of Agro-Food Science and Technology, Shandong Academy of Agricultural Sciences, Jinan 250100, China*

[2] *College of Food Science and Technology, Yunnan Agricultural University, Kunming 650201, China*

[3] *Medical Science and Technology Innovation Center, Shandong First Medical University & Shandong Academy of Medical Sciences, Jinan 250117, China*

[4] *Sports & Medicine Integration Research Center (SMIRC) Capital University of Physical Education and Sports, Beijing, 100191, China*

ABSTRACT: Designing food microstructures to elicit specific physiological responses is crucial for advancing functional food innovation. Pickering emulsions were fabricated using starch nanoparticles with tailored amylose/amylopectin ratios, prepared by blending modified high-amylose (HAMG) and waxy maize (WMG) starch granules. Increasing amylopectin content progressively reduced droplet size, shifting from a unimodal distribution centered at 13.76 μm in pure HAMG systems to predominantly smaller droplets (~1.72 μm) in pure WMG emulsions. *In vitro* digestion demonstrated that amylose-rich emulsions preserved higher structural integrity and suppressed lipid hydrolysis via a more rigid interfacial barrier, whereas amylopectin-rich emulsions enhanced enzyme accessibility and free fatty acid release. *In vivo* murine studies further demonstrated that high-amylose Pickering emulsions delayed gastric emptying and reduced postprandial plasma triglyceride levels. Duodenal transcriptomic analysis revealed that rapid lipid flux in WMG-treated mice induced pronounced metabolic reprogramming, including upregulation of genes involved in fatty acid transport (*fabp1/2*), chylomicron assembly (*apoa4*), peroxisomal β-oxidation (*acox2*), mitochondrial oxidative phosphorylation, and immune-related pathways. Overall, these results demonstrate that interfacial engineering using starch particles enables precise regulation of lipid digestion and intestinal metabolic responses, providing a rational strategy for targeted functional and medical food design.

Keywords: Maize Starch; Pickering emulsion; Lipid Digestion; Duodenum transcriptome; Energy metabolism; Immune function.

1. Introduction

A comprehensive understanding of the relationship between the food matrix and its digestion and absorption, as well as the impact of food structure and properties on the host's metabolic, immune, and other biological functions, is essential for the rational design and production of foods with enhanced nutritional characteristics [1]. This knowledge is crucial for designing food matrices by integrating various compositions,

[#] These authors contributed equally to this work
***Corresponding author**
Wei Liu, Email: 980701611@qq.com; Lingfei Li, Email: lingfeili@163.com.

Received 13 August 2025
Received in revised from 3 October 2025
Accepted 6 March 2026

structures, and properties to encapsulate bioactive components, thereby facilitating their release at specific sites within the gastrointestinal tract and enhancing their bioavailability [1]. Furthermore, modulating the characteristics of food matrices can improve or decrease the digestibility and absorption of macronutrients or micronutrients, laying the groundwork for the development of targeted nutritional supplements and functional foods [1, 2].

Lipids are essential macronutrients for the human body, providing energy and essential fatty acids, maintaining the structure of biological membranes, playing a crucial role in signal transduction, and serving as carriers for fat-soluble vitamins such as A, D, E, and K [3, 4]. However, imbalanced lipid intake and metabolic disorders are linked to various diseases, including obesity, diabetes, fatty liver, cardiovascular diseases, cancer, and mental health conditions such as depression and anxiety [5, 6]. Variations in lipids and their hydrolysis products in the digestive tract determine the processes of lipid uptake, transport, and reassembly into chylomicrons in the small intestine, thereby influencing postprandial lipid levels and systemic lipid homeostasis [7]. Additionally, as a key organ in lipid sensing and metabolism, the small intestine's interaction with lipids and their hydrolysis products can activate metabolic and sensing pathways, triggering systemic biological responses that may profoundly affect metabolism [8], immunity [9], and endocrine function [10]. Designing food matrices to regulate lipid digestion, absorption, and metabolism in a controlled manner may represent a strategy to mitigate lipid-related disorders [11].

In most processed foods, lipids primarily exist in emulsified forms, either as final products or as components within more complex food systems, such as mayonnaise, salad dressings, and ice cream [3]. Studies have shown that droplet size, emulsifier composition, and the rheological properties of emulsion systems significantly influence lipid digestion and absorption within the gastrointestinal tract [12]. For example, the binding of lipase to the surface of oil or fat droplets in emulsions represents the initial step in lipid hydrolysis. The droplet size critically influences this binding and the subsequent enzymatic activity, thereby altering the rate of lipid hydrolysis [13]. Additionally, the selection of emulsifiers and other components in the emulsion system significantly influences the adsorption of lipase and co-lipase onto the surface of lipid droplets [14]. Moreover, the rheological properties of foods, such as viscosity, can modulate lipid digestion and absorption by influencing gastric emptying rates [15]. Thus, adjusting the composition and structure of emulsions can tailor lipid release within the gastrointestinal tract, allowing for enhanced control over lipid digestion and absorption. A deeper understanding of how the digestive system processes, transports, and utilizes lipids could enable the microstructural design of foods to achieve specific, controlled physiological outcomes.

Traditional emulsions have typically relied on synthetic surfactants or animal-derived emulsifiers, both of which are unsustainable due to their negative environmental impact [16]. Additionally, the adverse effects of commonly used emulsifiers in traditional emulsions on gut microbiota and intestinal health have drawn increasing attention [17]. In this context, Pickering emulsions, stabilized by solid particles such as inorganic materials or biopolymers, present a viable alternative to conventional surfactants. As a result, natural

biopolymers such as starch are being increasingly utilized in Pickering emulsions [18, 19]. The structure and properties of native starches from different plant sources vary significantly, and starches from sources such as maize, potato, and quinoa have demonstrated applicability in Pickering emulsions [20]. Notably, maize starch represents a uniquely powerful and versatile model system because of the commercial availability of genetically well-defined variants with extreme differences in amylose content, namely high-amylose maize starch (>50% amylose) and waxy maize starch (<2% amylose) [21]. By physically blending these two starches, the amylose-to-amylopectin ratio can be continuously and precisely adjusted over a broad range (approximately 2%–70% amylose), enabling a level of compositional control that is difficult to achieve with starches from other botanical sources, whose amylose contents are typically confined to relatively narrow genetic ranges[21-23].

Previous studies have demonstrated that variations in starch particle characteristics and preparation methods can substantially influence the particle size, rheological behavior, interfacial properties, and stability of starch-stabilized Pickering emulsions, thereby affecting their functional performance [24]. Owing to their natural origin, high biodegradability, and low toxicity, starch-based Pickering emulsions are particularly attractive for food and health-related applications [25]. Nevertheless, existing research has largely focused on comparing emulsifying performance among different starch types or modification strategies, while the fundamental role of the amylose-to-amylopectin ratio as a primary molecular determinant has not been systematically elucidated. Specifically, a clear causal framework linking starch molecular composition to interfacial architecture, emulsion microstructure, digestive behavior, and downstream physiological responses remains lacking. In particular, how variations in the amylose-to-amylopectin ratio regulate lipid digestion and absorption kinetics, and whether these effects further translate into changes in intestinal metabolic signaling and transcriptomic responses, have not been comprehensively investigated. Addressing this knowledge gap is essential for the rational design of starch-based Pickering emulsions with targeted nutritional and health functions.

In this study, we hypothesize that the amylose-to-amylopectin ratio of maize starch granules governs the interfacial architecture and stability of starch-based Pickering emulsions, thereby modulating lipid digestion and absorption behavior in the gastrointestinal tract. To address this hypothesis, starch particles with varied amylose/amylopectin ratios were prepared via an anti-solvent modification strategy using high-amylose and waxy maize starches and subsequently employed to fabricate Pickering emulsions by ultrasonic treatment. The physicochemical properties of the resulting emulsions and their lipolysis kinetics during simulated gastrointestinal digestion were comprehensively evaluated. Furthermore, a mouse model was used to investigate how emulsion structural variations influence gastrointestinal digestive behavior, postprandial lipid responses, and transcriptomic alterations in the small intestine. Collectively, this study elucidates the structure-digestion-response relationships of starch-based Pickering emulsions and provides mechanistic insights for the rational design of starch particle-stabilized emulsions with programmable lipid release and metabolic modulation in the gastrointestinal tract.

2. Materials and Methods

2.1. Materials

High-amylose maize starch and waxy maize starch were sourced from Ingredion (Bridgewater, NJ, USA), while sunflower oil was obtained from a local market. Total cholesterol (TC) and total triglyceride (TG) assay kits were procured from Nanjing Jiancheng Bioengineering Institute (Nanjing, Jiangsu, China). Free fatty acids (FFAs), triacylglycerols (TAGs), vitamin D3, pepsin, trypsin, pig bile salts, acetonitrile, and isopropanol were purchased from Sigma-Aldrich Co. (St. Louis, MO, USA). Pancreatin was obtained from Aladdin Biological Technology Co. (Shanghai, China). All other chemicals utilized in this study were of analytical grade.

2.2. Preparation and characterization of starch granules

2.2.1. Preparation of starch granules

Starch granules derived from high-amylose maize starch and waxy maize starch were prepared following the anti-solvent method described by Yan et al. [26], with slight modifications. A 5% (w/v) starch suspension was stirred at 70°C for 1 hour. An equal volume of ethanol was subsequently added to the starch suspension. The mixture was centrifuged at 3000 × g for 10 min to separate the precipitate, which was collected and vacuum freeze-dried. The resulting high-amylose maize starch granules (HAMG) and waxy maize starch granules (WMG) were then used for further analysis and emulsion preparation.

2.2.2. Scanning electron microscopy of starch granules

HAMG and WMG samples were mounted on conductive adhesive and coated with a thin layer of gold using a Quorum SC7620 sputter coater for 45 seconds at a current of 10 mA. The morphology and elemental composition of the samples were examined using a TESCAN MIRA LMS scanning electron microscope (SEM). An acceleration voltage of 3 kV was used for imaging sample morphology, while 15 kV was applied for elemental mapping. Imaging was conducted using an SE2 secondary electron detector.

2.2.3. Particle size analysis

The particle size distributions of HAMG and WMG were determined using a laser particle size analyzer (BT-2001, Dandong Bettersize Instruments Ltd., China). For analysis, each sample was dispersed in a measurement cell containing 500 mL of deionized water, with continuous stirring. The dispersion process was maintained until light obscuration reached 10-15%, a threshold established to minimize multiple scattering effects. The average particle size was expressed as the volume-weighted mean diameter ($D_{4,3}$) and the surface-weighted mean diameter ($D_{3,2}$).

2.2.4. Amylose/Amylopectin content

The amylose and amylopectin contents were analyzed in the original starch samples, including high-amylose maize starch and waxy maize starch, as well as in the treated starch particles (HAMG and WMG) and the resulting Pickering emulsions. Detailed analytical methods and corresponding results are presented in the supplementary materials.

2.3. Preparation and characterization of Pickering emulsions with different Amylose/Amylopectin ratios

2.3.1. Preparation of Pickering emulsion

Pickering emulsions were prepared according to a previously reported method with minor modifications [27]. A 5% (w/v) starch suspension was mixed with sunflower oil at a 4:1 (v/v) ratio and homogenized at 13,000 rpm for 2 min using an IKA T25 high-speed homogenizer (Staufen, Germany). The resulting emulsion was sonicated for 3 min at 500 W using an ultrasonic processor (20 kHz, maximum power: 500 W, Sonics & Materials Inc., USA) to produce the final Pickering emulsion.

2.3.2. Particle size

The particle size analysis of the Pickering emulsions was conducted using a BT-2001 laser particle size analyzer (Dandong Bettersize Instruments Ltd., China), following the procedure outlined above for starch particle size measurement.

2.3.3. Microscopic observation

The microstructure of the Pickering emulsion was analyzed using a Thermo Fisher Scientific EVOS M7000 fluorescence microscope (USA). Optical images of the emulsions were captured using the bright-field mode of the microscope. To enhance the visualization of oil droplets within the emulsion, 100 μL of the emulsion was stained with 1 μL of Nile Red solution (0.1 mg/mL). Fluorescence microscopy imaging was conducted using an excitation wavelength of 488 nm, with emitted fluorescence collected at 650 nm. Starch particles in the Pickering emulsions were stained with Calcofluor White and visualized using a Nikon A1R HD25 Confocal Laser Scanning Microscopy (CLSM, Nikon, USA). The excitation wavelength was set at 405 nm, and the emission signal was collected at 445 nm.

2.3.4. Molecular dynamics simulations

Molecular dynamics (MD) simulations were employed to investigate the interfacial assembly and stabilization mechanisms of starch particles at the molecular scale. All simulations were performed using the GROMACS simulation package (version 2024.2) in conjunction with the CHARMM36 force field, following the general protocol proposed by Ke et al. [28].

The simulation models were designed to mimic an oil–water interfacial system, consisting of starch granules with different amylose-to-amylopectin ratios, triolein molecules representing the lipid phase, and explicit water molecules enclosed within a three-dimensional periodic simulation box. Prior to the production runs, each system was subjected to an energy minimization procedure lasting 500 ps to remove unfavorable atomic contacts, followed by sequential equilibration under constant-volume and constant-temperature (NVT) conditions for 5 ns and constant-pressure and constant-temperature (NPT) conditions for an additional 5 ns.

After satisfactory equilibration was confirmed, a 20 ns production MD simulation was conducted for each system. GPU acceleration based on CUDA technology was applied to improve computational efficiency. The resulting trajectories were subsequently analyzed to quantify hydrogen bonding interactions between starch granules with different structural compositions and lipid molecules at the oil–water interface.

2.4. In vitro simulated gastrointestinal digestion of Pickering Emulsion

In vitro simulated gastrointestinal digestion was conducted in accordance with the standardized INFOGEST protocol proposed by Brodkorb *et al.* [29]. In the simulated gastric digestion phase, the emulsion was mixed with simulated gastric fluid in a 1:1 volume-to-volume ratio and incubated at 37°C with shaking at 120 rpm for 2 hours. The pH of the system was carefully adjusted to 3.0 using 0.1 mol/L HCl. Pepsin and lipase were added at final concentrations of 2000 U/mL and 60 U/mL, respectively. In the subsequent intestinal digestion phase, the gastric digestate was mixed with simulated intestinal fluid in a 1:1 volume-to-volume ratio and incubated at 37°C with shaking at 120 rpm for another 2 hours. The pH of the system was adjusted to 7.0 using 0.1 mol/L NaOH. Pancreatin and bile salts were added at final concentrations of 100 U/mL (based on trypsin activity) and 10 mmol/L, respectively. The compositions of the simulated gastric and intestinal fluids are listed in Table S1 (Supplementary Materials). After each digestion phase, the reaction mixtures were heated in boiling water for 5 min to inactivate the enzymes.

2.5. Free fatty acids analysis during simulated digestion process

The FFAs content variation was assessed following the method described by Marefati et al., with minor modifications [30]. During the *in vitro* simulated gastrointestinal digestion, samples were collected from both the gastric and intestinal phases at intervals of 0, 5, 10, 15, 20, 30, 40, 60, 80, 100, and 120 min. The pH of each sample was adjusted to 7.0 using NaOH, and the volume and concentration of NaOH required for the adjustment were recorded.

To correct for background free fatty acids (FFAs) inherently present in the oil phase, parallel blank experiments were performed using undigested sunflower oil under identical conditions. The average NaOH consumption attributable to background FFAs was defined as V_{Blank} and subtracted from all titration volumes prior to FFA calculation [31]. The V_{Blank} value determined for the emulsions in this study was 46 μL. Furthermore, to correct for the incomplete ionization of medium-chain FFAs at pH 7.0, a titration endpoint correction factor was determined following a previously reported method [29, 32]. Briefly, representative sunflower oil samples were titrated to pH 7.0 and pH 10.0 using 0.1 mol/L NaOH, and the ratio of NaOH volumes consumed was used to calculate an average correction factor (CF_{Final} = 1.67).

The release of FFAs was calculated using the method described by Nikbakht et al [33], with V_{Blank} and CF_{Final} applied as described above.

$$FFA\ (\%) = \frac{(V_{NaOH} - V_{Blank}) \times C_{NaOH} \times M_{Lipid} \times CF_{Final}}{2 \times W_{Lipid}}$$

Where V_{NaOH} is the volume of NaOH consumed to reach pH 7.0 (mL), C_{NaOH} is the concentration of NaOH (mol/mL), M_{Lipid} is the molecular weight of sunflower oil, approximated based on its main component, triolein (M=885.4 g/mol), W_{Lipid} is the mass of oil in the system (g), and the factor 2 indicates that an average of two molecules of NaOH are required to release one molecule of FFA from a triglyceride.

2.6. Animal study

Seventy-five male ICR mice, aged 12–14 weeks, were procured from Pengyue Laboratory Animal Breeding Co., Ltd. (Ji'nan, Shandong, China). The animal protocol was approved by the Ethics Committee of

Yunnan Agricultural University (approval number 202409001). The mice were housed under controlled conditions at a temperature of 22 ± 2 °C, with a relative humidity of 50%–60%, and maintained on a 12-hour light/dark cycle. They had ad libitum access to water and a standard rodent chow diet. Based on the divergent *in vitro* lipolysis profiles reported in Sections 3.3 and 3.4, three Pickering emulsions with contrasting amylose/amylopectin ratios were selected for *in vivo* study. This selection encompasses a representative range of interfacial stabilities, from highly digestion-resistant to readily bioaccessible systems. Following an 18-hour fasting period, the mice were randomly assigned to five weight-matched groups (n = 15) and administered one of the following emulsions or distilled water via gavage: 1) Pickering emulsion stabilized with HAMG (HAMG group); 2) Pickering emulsion stabilized with WMG (WMG group); 3) Pickering emulsion stabilized with a 1:1 mixture of HAMG and WMG (HAMG/WMG group); 4) a mixture of sunflower seed oil and distilled water (SOW group); and 5) distilled water (CTRL group).

After oral gavage, mice were euthanized at 1, 2, and 4 h post-administration, and relevant tissues were immediately collected for subsequent analyses. The number of mice at each time point was predetermined based on experimental requirements, with four mice per group at 1 and 2 h and seven mice per group at 4 h, the latter being necessary to ensure sufficient plasma sample size for downstream biochemical analyses.

Blood samples were collected from a designated subgroup of mice at the 4 h time point. Prior to euthanasia, blood was obtained from the tail vein into EDTA-coated tubes at baseline (0 h) and at 1, 2, 3, and 4 h post-gavage. Plasma was separated by centrifugation at 2,500 × g for 10 min at 4 °C and stored at −80 °C until further analysis.

2.7. Tissue collection

Mice were anesthetized with isoflurane and subsequently euthanized by cervical dislocation at 1, 2, and 4 h post-gavage. Following abdominal cavity opening, the stomach and small intestine were isolated. The small intestine was divided into equal upper, middle, and lower segments, and the contents from each segment were collected for fluorescence microscopy analysis. For transcriptome analysis, a 2 cm segment of the proximal duodenum, immediately distal to the pyloric sphincter, was excised from mice euthanized 1 h post-gavage. The collected samples included the full thickness of the duodenal wall, encompassing the mucosal, submucosal, and muscular layers. Duodenal tissues were immediately snap-frozen in liquid nitrogen and stored at −80 °C until RNA extraction.

2.8. Fluorescence microscopy observation of lipids in the gastrointestinal contents

The stomach and small intestine contents were mixed with PBS solution at a 1:1 (w/v) ratio and stained with Nile red (1 mg/mL) at one-tenth the volume of PBS. The top layer was collected for fluorescence microscopy observation following centrifugation at 2,350 ×g for 10 min.

2.9. Analysis of triglycerides and free fatty acids in the gastrointestinal contents

The gastrointestinal contents were weighed, lyophilized, and the lipids were extracted using a modified Folch method, followed by analysis via high-performance liquid chromatography (HPLC) to quantify TAGs

and FFAs, as previously described [34, 35]. Vitamin D3 (100 μg/mL) was used as the internal standard. Chromatographic conditions were as follows: the HPLC system (1260, Agilent Technologies, USA) was equipped with a variable wavelength detector (VWD) and a Hypersil GOLD C18 column (4.6 × 250 mm, 5 μm, Thermo Scientific). The column temperature was maintained at 25°C. The injection volume was set to 10 μL, with a flow rate of 1 mL/min. The mobile phase comprised isopropanol and acetonitrile, applied in isocratic elution mode. The isocratic elution program was set as follows: 0-30 min, 60% acetonitrile. The detection wavelength was set to 205 nm.

2.10. Plasma lipid determination

Plasma total triglycerides (TG) and total cholesterol (TC) levels were measured with commercial kits following the procedures outlined in the instruction manual.

2.11. Comparative analysis of transcriptome profiling data of duodenum tissue

Total RNA was isolated from duodenal tissue (n=4 per group) using TRIzol® Reagent (Invitrogen) following the manufacturer's protocol. DNase I (Takara) treatment was used to eliminate genomic DNA contamination. The quality and quantity of RNA samples were evaluated using agarose gel electrophoresis, NanoDrop2000 (NanoDrop Technologies), and the 5300 Bioanalyzer (Agilent Technologies). Only high-quality RNA samples were selected for library construction. Purified and reverse-transcribed RNA samples were sent to Shanghai Majorbio Bio-pharm Biotechnology Co., Ltd. (Shanghai, China) for library preparation and sequencing on an Illumina Novaseq 6000 platform (paired-end, 2×150 bp) following the manufacturer's guidelines (Illumina, San Diego, CA). Raw paired-end reads were trimmed, quality-checked, and the resulting clean reads were aligned to the Mus musculus reference genome. Following the assessment of mapping results, transcripts were assembled and annotated using Cufflinks StringTie (https://ccb.jhu.edu/software/stringtie/). Transcript expression levels were quantified using the transcripts per million (TPM) method [36]. Differential expression analysis was conducted using the DESeq2 package [37, 38]. Genes exhibiting an absolute logarithmic fold change ($|\log_2 FC| \geq 1$ and a false discovery rate (FDR) $\leq$ 0.05 were defined as differentially expressed genes (DEGs). Functional enrichment analysis of differentially expressed genes was subsequently performed based on the Kyoto Encyclopedia of Genes and Genomes (KEGG) database using KOBAS[39] to identify significantly enriched metabolic and signaling pathways.

2.12. Statistical analysis

Statistical analysis was performed using one-way ANOVA or student's t-test with GraphPad Prism software (version 10.1.2, GraphPad Software, Inc., La Jolla, California). A difference is considered statistically significant when the $P < 0.05$. Data are expressed as means ± SEM.

3. Results and discussion

3.1. Properties of Pickering emulsions stabilized by varying Amylose/Amylopectin ratios

Starch nanoparticles were intended to be prepared using the anti-solvent method for application in the fabrication of Pickering emulsions. However, in practice, high-amylose starch retrogrades rapidly after being

heated to its gelatinization temperature, making process control challenging. To address this, waxy maize starch was heated above its gelatinization temperature, whereas high-amylose starch was heated only to a temperature suitable for partial gelatinization, followed by ultrasonication to prepare Pickering emulsions. After treatment in a 70 °C water bath and subsequent ethanol precipitation, both untreated and pretreated starch samples were used for emulsion preparation. As shown in Fig. S1 (Supplementary Materials), emulsions prepared with untreated raw starch failed to form a stable emulsion system, whereas all pretreated starch samples, when combined with ultrasonication, successfully formed stable emulsions.

The morphologies of the high-amylose maize starch granules (HAMG) and waxy maize starch granules (WMG) were characterized by scanning electron microscopy (SEM) (Fig. 1, A-B). HAMG exhibited relatively regular granule morphologies with smooth surfaces, whereas WMG showed more irregular shapes and notably rougher surfaces. This roughness is likely attributable to granule aggregation mediated by intermolecular hydrogen bonding among surface hydroxyl groups[40]. Particle size analysis (Fig. 1, C -D) confirmed the aggregation levels of starch granules as illustrated by SEM observations. HAMG particles ranged in size from 0.5 μm to 306.9 μm, with a peak at 15.3 μm, whereas WMG particle sizes ranged from 1.6 μm to 161.4 μm, peaking at 32.1 μm. It should be noted that the morphologies and particle size distributions reported here represent the pre-emulsification state of the starch granules and may not fully reflect their structural characteristics within the final emulsions, as substantial granule fragmentation and restructuring can occur during subsequent ultrasonication. This limitation has been acknowledged in the interpretation of the results.

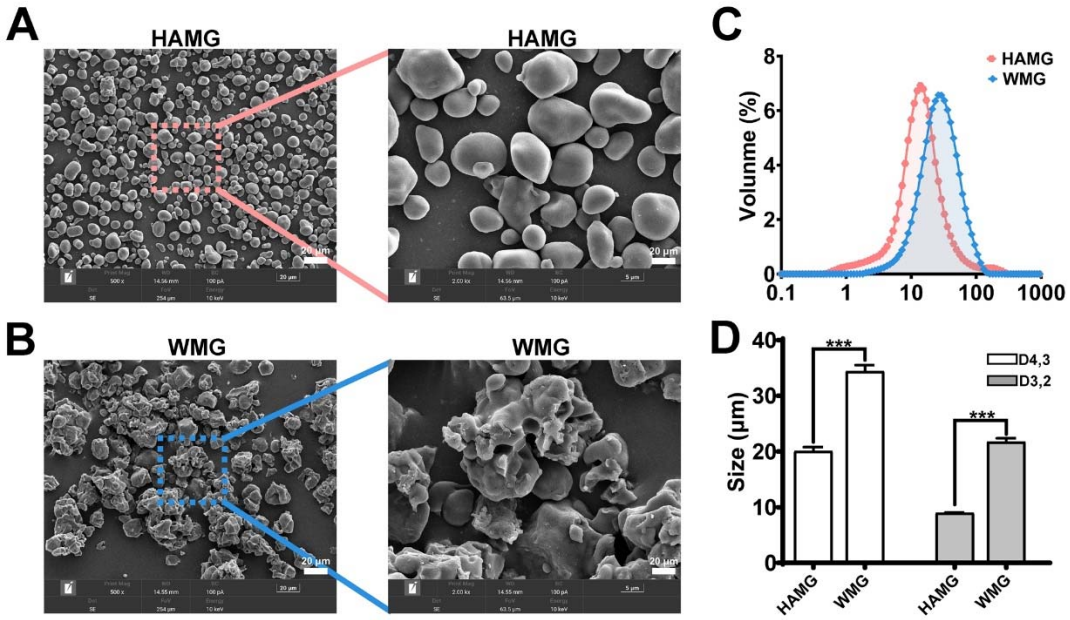

Fig. 1. Scanning electron micrographs of (A) HAMG and (B) WAG; (C) Starch particle size distribution range; (D) the average particle size in terms of the volume-weighted mean diameter $D_{4,3}$ and the surface-weighted mean diameter $D_{3,2}$. HAMG: high amylose maize starch granules; WMG: waxy maize starch granules.

As shown in Table S2, the prepared HAMG consists of 81.16% amylose and 18.84% amylopectin, whereas WMG comprises 6.64% amylose and 93.36% amylopectin. By blending WMG and HAMG in various ratios, we generated starch granule materials with distinct amylose/amylopectin compositions, which

were then utilized for the preparation of emulsions. Specific ratios of HAMG to WMG (1:0, 2:1, 1:1, 1:2, 0:1) yielded samples with distinct gradients in amylose and amylopectin content. Emulsions derived from pure HAMG (1:0) were 71.29% amylose and 28.71% amylopectin, while those from WMG (0:1) were 9.51% amylose and 90.49% amylopectin, reflecting slight discrepancies from the original starch compositions. This variation may be due to structural changes during emulsion preparation via ultrasonication or due to differences in the analyzed sample state. Starch granules prepared at a 2:1 HAMG to WMG ratio contained 46.99% amylose and 53.01% amylopectin. In mixtures with HAMG to WMG ratios of 1:1 and 1:2, the proportions of amylose and amylopectin were more balanced, with amylose contents of 42.57% and 31.20%, and amylopectin contents of 57.43% and 68.80%, respectively. As the proportion of WMG increased, the amylopectin content in the starch granule mixtures progressively increased, while the amylose content correspondingly decreased.

Pickering emulsions were prepared using starch granules with varying amylose contents, achieved by blending high-amylose maize granules (HAMG) and waxy amylopectin granules (WMG) in different proportions. Consistent with previous studies, dual-fluorescence labeling combined with CLSM observation (Fig. S2) confirmed the formation of starch-based oil-in-water Pickering emulsions, as evidenced by the clear localization of starch granules at the oil-water interface [20]. As shown in Fig. 2, stable emulsions were formed at various amylose-to-amylopectin ratios, leading to distinct microstructures. Microscopic analysis revealed that emulsions formed with pure HAMG (HAMG: WMG = 1:0) exhibited the largest droplet sizes. As the amylose content in the starch granules decreased and the amylopectin content increased, a clear trend of droplet size reduction was observed. The smallest droplet sizes were observed in Pickering emulsions formed with pure WMG (HAMG: WMG = 0:1).

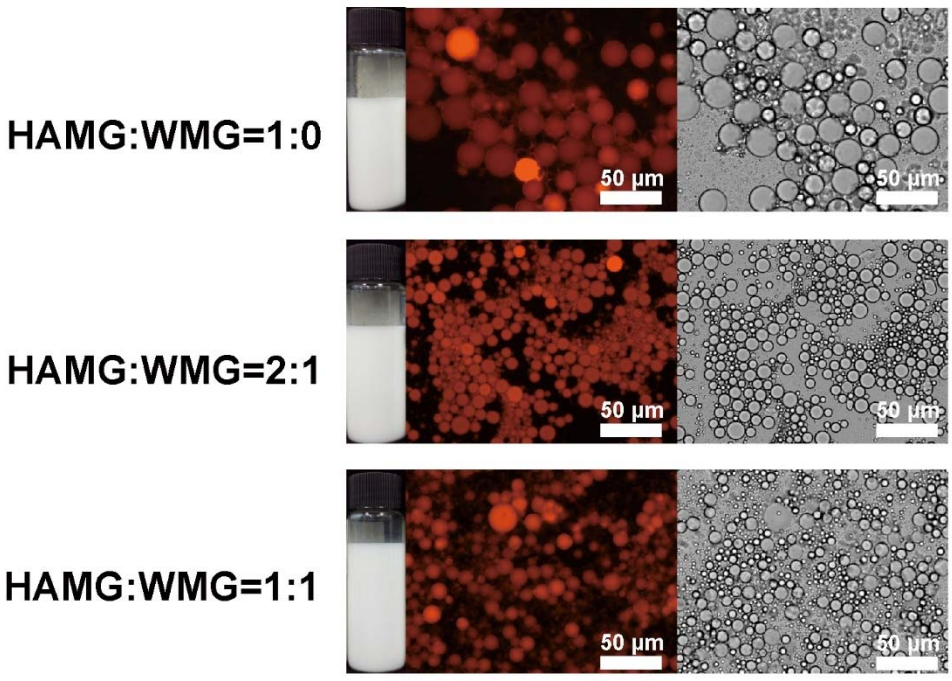

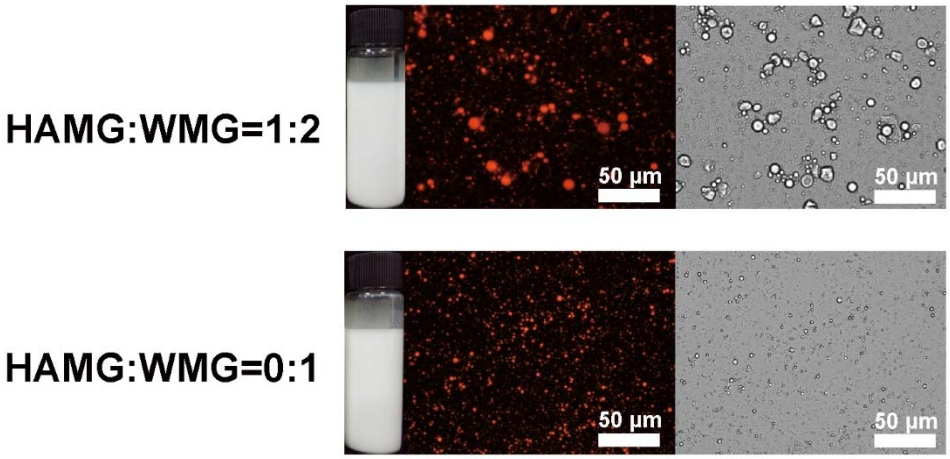

Fig. 2. Photographs, optical microscopy images, and fluorescence microscopy images of Pickering emulsions stabilized with varying amylose/amylopectin ratios.

Particle size analysis results illustrated in Fig. 3 corroborates these microscopic observations. As shown in Fig. 3A, the Pickering emulsion stabilized by HAMG has only one peak, with a particle size of 13.76 μm. With the addition of WMG, at a HAMG: WMG ratio of 2:1, besides the original peak at 13.76 μm, a peak with a particle size of 1.72 μm appears. As the proportion of WMG continues to increase, the proportion of smaller droplets also increases. In the emulsion stabilized by pure WMG, the smaller droplets (around 1.72 μm) dominate the emulsion system. This trend is further supported by the statistical analysis of droplet sizes, $D_{4,3}$ and $D_{3,2}$, as shown in Fig. 3B. Interestingly, the droplet sizes in emulsions formed by starch particles were unexpectedly smaller than the starch particle sizes themselves. This phenomenon may arise from the disruption of starch aggregates-initially detected by laser diffraction-into smaller functional units under the intense shear and ultrasonic forces applied during emulsification [41].

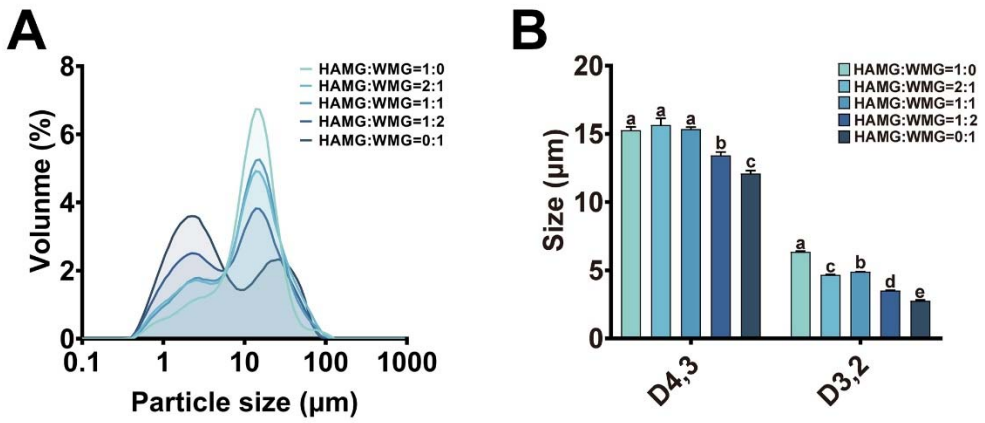

Fig. 3. (A) Particle size distribution, and (B) the average particle size in terms of the $D_{4,3}$ and the $D_{3,2}$ of Pickering emulsions stabilized with varying amylose/amylopectin ratios. Different letters indicate significant differences ($P < 0.05$).

The inherent physicochemical properties of starch particles play a critical role in determining their interfacial behavior [20, 42]. Lu *et al*. demonstrated that milling-induced nano-starch particles with varying amylose contents resulted in distinct rheological and stability profiles [27]. Aligned with these observations, the present study identified a similar correlation where a higher amylopectin content (represented by a higher

WMG ratio) led to a reduction in average droplet size. These results establish a well-defined model for exploring the interplay between emulsion architecture and subsequent lipid digestion.

3.2. Molecular dynamics of Pickering emulsions stabilized by different Amylose/Amylopectin ratios

The stabilization of Pickering emulsions by starch granules potentially involves a multiscale synergistic mechanism. Starch particles undergo irreversible adsorption at the oil–water interface, establishing a robust mechanical barrier against coalescence [43]. Simultaneously, the formation of a three-dimensional network within the continuous phase provides structural scaffolding that physically imprisons the oil droplets [44]. Furthermore, the stability is locally enhanced by steric hindrance and electrostatic repulsion, which collectively prevent droplet aggregation [45, 46].

To further elucidate the stabilization mechanism at the molecular level, molecular dynamics (MD) simulations were performed to monitor the interfacial morphological evolution and hydrogen-bonding (H-bond) behavior of starch particles at the oil–water interface (Fig. 4). As shown in Fig. 4A, regardless of the mass ratio, both high-amylose maize starch (HAMG, red) and waxy maize starch (WMG, orange) spontaneously migrated from the bulk phase and became anchored at the biphasic interface within 20 ns of simulation. This spontaneous adsorption process provides direct molecular-level evidence for the thermodynamically favorable interfacial affinity of starch particles as Pickering stabilizers.

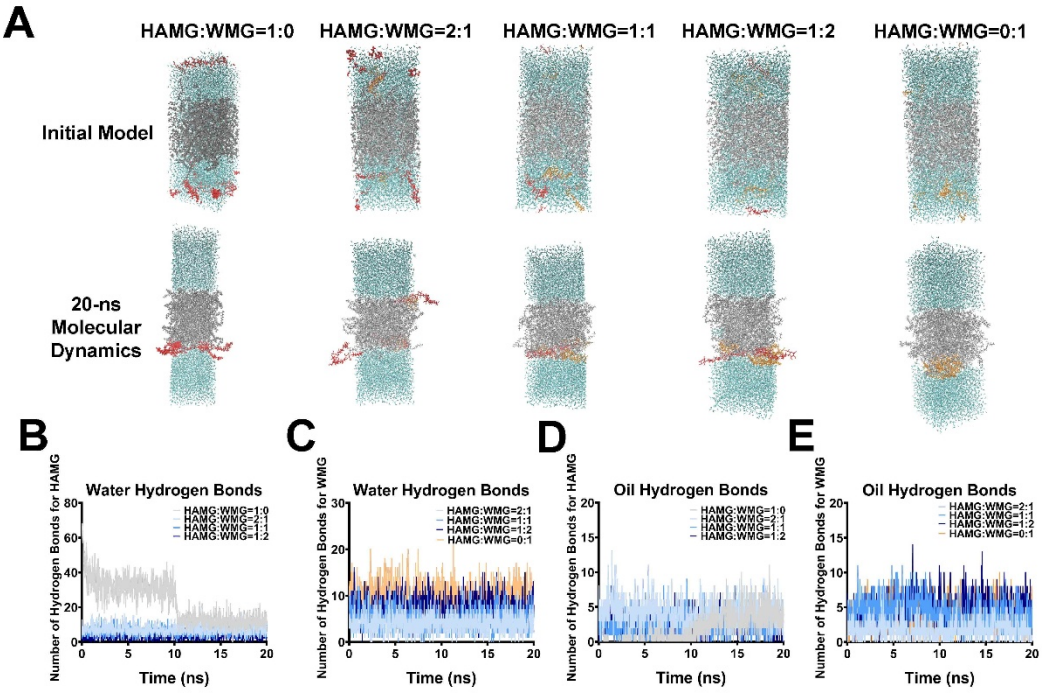

Fig. 4. Morphological evolution and hydrogen bond behavior of Pickering emulsions stabilized by HAMG-WMG starch blends with different mass ratios during molecular dynamics simulations. (A) Morphological evolution of Pickering emulsions stabilized by HAMG-WMG blends (mass ratios = 1:0, 2:1, 1:1, 1:2, and 0:1) from the initial model to 20-ns molecular dynamics (MD) simulation. The gray region represents the oil phase, light blue represents the aqueous phase, red represents HAMG, and orange represents WMG. (B, C) Time-dependent number of hydrogen bonds between starch (HAMG in B, WMG in C) and water molecules during 20-ns MD simulation. (D, E) Time-dependent number of hydrogen bonds between starch (HAMG in D, WMG in E) and oil-phase molecules during 20-ns MD simulation.

Quantitative analysis of hydrogen-bonding dynamics further elucidated the interfacial transition process. For the HAMG system (Fig. 4B and D), a pronounced crossover point was observed at approximately 10 ns, at

which the number of hydrogen bonds formed between starch molecules and water decreased sharply, while hydrogen bonding with the oil phase increased markedly. This abrupt transition quantitatively captures the energetic gain associated with overcoming the hydration barrier, enabling the irreversible adsorption of starch particles at the interface. Notably, compared with HAMG, WMG established hydrogen bonds with oil molecules at an earlier stage and in a more stable manner (Fig. 4E), indicating a higher interfacial affinity and faster interfacial spreading kinetics. This molecular behavior provides a mechanistic explanation for the experimentally observed reduction in emulsion droplet size with increasing amylopectin content, as the branched architecture facilitates more rapid and denser interfacial coverage, thereby effectively suppressing droplet coalescence during homogenization [27, 47].

These findings support the multilevel stabilization model proposed in this study. Specifically, the compact interfacial layer observed in the MD simulations functions as a mechanical barrier (shielding effect), while the extensive hydrogen-bonding network between starch particles reinforces a three-dimensional gel structure within the continuous phase. Such a hierarchical stabilization mechanism, underpinned by the high desorption energy of particles adsorbed at the oil–water interface, has been widely recognized as a key factor governing the storage stability of Pickering emulsions [43, 48].

In addition, a 15-day storage study was conducted to evaluate the stability of the formulated emulsions. As shown in Fig. S3, all emulsions remained physically stable throughout the storage period, only the emulsion stabilized by pure HAMG (HAMG: WMG = 1:0) exhibited slight phase separation, which is consistent with its comparatively larger droplet size observed previously. The poorer storage stability of the HAMG-stabilized emulsion arises from its larger droplet size and less compact interfacial structure, whereas WMG facilitates rapid interfacial adsorption and denser particle packing, in agreement with the MD simulations, thereby improving resistance to droplet coalescence and phase separation during storage [49].

3.3. In vitro simulated digestion of Pickering emulsion stabilized by different ratios of Amylose/Amylopectin

To investigate the fate of Pickering emulsions stabilized by varying amylose/amylopectin ratios after ingestion, *in vitro* simulated gastrointestinal digestion was performed. The results are summarized in Fig. 5. As shown in the Nile red staining results of lipid droplets in digestive fluids at different stages (Fig. 5A), the lipid droplets in the gastric phase were relatively stable, with significant aggregation occurring only in the two groups with higher amylopectin content (HAMG/WMG = 1:2, 0:1). Consistent with fluorescent microscopy observations, particle size measurements (Fig. 5B) indicated that compared to the initial droplet sizes, the groups with higher amylose content (HAMG/WMG ratios of 1:0, 2:1, and 1:1) exhibited no significant changes in droplet size. In contrast, the amylopectin-dominated groups (HAMG/WMG ratios of 1:2 and 0:1) showed a noticeable increase in droplet size, suggesting that flocculation or coalescence had occurred [50].

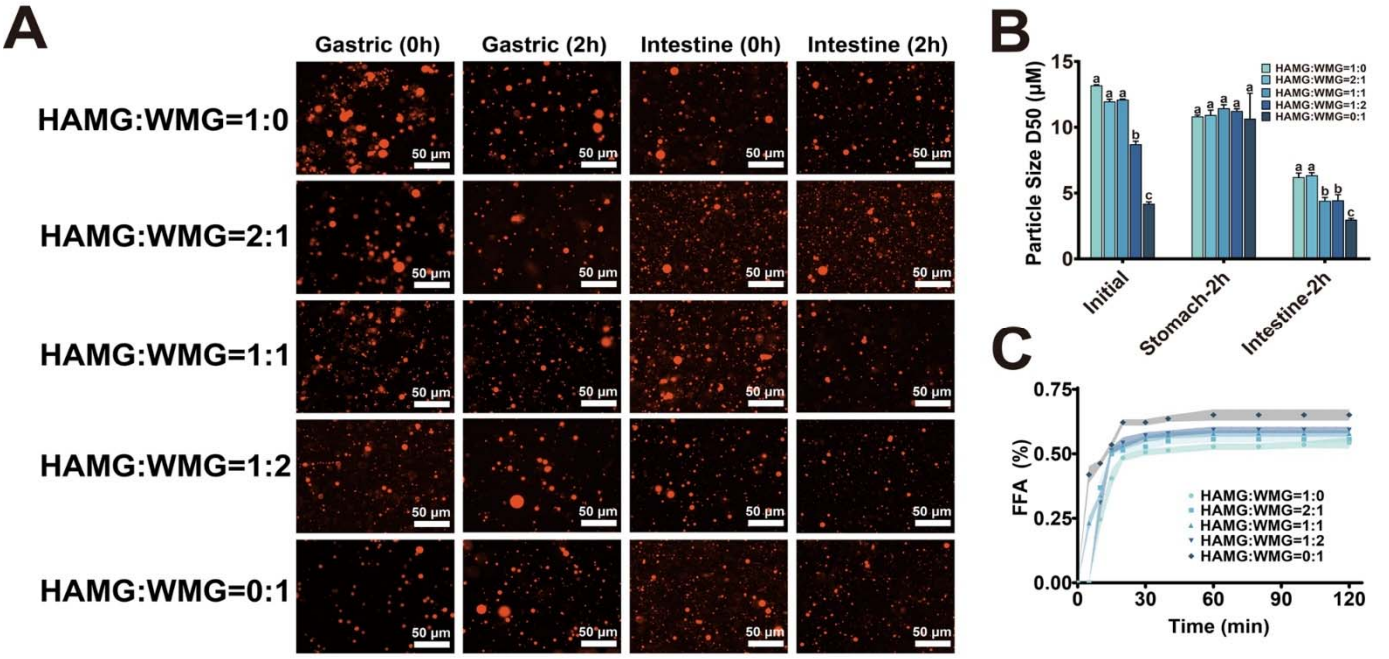

Fig. 5. (A) Fluorescence microscopy morphology, and (B) changes in the particle size of Pickering emulsions stabilized with varying amylose/amylopectin ratios during gastric, and intestinal phases in *in vitro* simulated digestion. (C) Release of free fatty acids (%) from the different Pickering emulsions during intestinal phase of *in vitro* simulated digestion. Different letters indicate significant differences ($P < 0.05$).

Particle size analysis revealed that after two hours of *in vitro* simulated intestinal digestion, the Pickering emulsion droplet size decreased significantly, primarily due to the hydrolysis of oil droplets. Fluorescence microscopy observations showed that by the end of intestinal digestion, most lipid droplets had been hydrolyzed. Fig. 5B further demonstrated a significant decrease in droplet size during the intestinal phase. Additionally, particle size analysis showed that at the end of *in vitro* intestinal digestion, a decreasing amylose-to-amylopectin ratio corresponded to a reduction in droplet size. The groups with HAMG/WMG ratios of 1:2 and 0:1 exhibited the smallest particle sizes, indicating that during the intestinal phase, the amylose-to-amylopectin ratio continued to influence the digestion extent of the Pickering emulsion. Higher amylopectin content resulted in more extensive degradation of both starch and lipid droplets in the emulsion.

The differences in digestibility between amylose and amylopectin in the digestive tract are largely determined by their molecular structures. During the simulated intestinal phase, amylopectin hydrolysis is markedly accelerated by pancreatic α-amylase, which aligns with the pronounced degradation of amylopectin observed under intestinal conditions (Fig. S4). Amylopectin's highly branched structure makes it more accessible to digestive enzymes [51]. The enzymatic breakdown of starch granules progressively reduces steric hindrance at the oil–water interface, thereby facilitating lipase–colipase adsorption and promoting lipid droplet hydrolysis [52].

In contrast, amylose, owing to its relatively linear chains and compact molecular packing, exhibits greater resistance to enzymatic penetration and consequently undergoes slower degradation [53]. It is noteworthy that the molecular structure of starch granules not only directly influences their enzymatic susceptibility but also modulates droplet size by determining the interfacial properties of the emulsion-the

rigidity of high-amylose starch granules promotes the formation of larger emulsion droplets [54]. Consequently, the observed differences in digestive behavior arise from the concerted effects of the molecular structural characteristics of starch and the resulting physical structure of the emulsion, particularly the droplet size. This structural difference explains the variations in particle size changes at different amylose/amylopectin ratios during the gastric phase of *in vitro* simulated digestion [50]. Overall, Pickering emulsions with higher amylose content exhibited enhanced structural integrity and reduced digestibility, reflecting the inherent resistance of amylose-rich systems and their associated emulsion architectures.

3.4. Release of free fatty acids during in vitro digestion of Pickering emulsions

In addition to the digestion of starch granules and their influence on droplet size during digestion, the breakdown of oil significantly impacts the nutritional value and potential applications of the emulsion. Based on the changes in emulsion particle size and droplet morphology observed under fluorescence microscopy, the oil phase in starch-stabilized emulsions primarily degrades during the intestinal phase of *in vitro* simulated digestion (Fig. 5A). This is expected, as the small intestine is the primary site for lipid digestion and absorption in the body. During this process, lipids, primarily triglycerides, are hydrolyzed into FFAs, diglycerides, monoglycerides, and glycerol [7]. These hydrolysis products are absorbed by intestinal epithelial cells, where they are further metabolized, transported, or utilized [7].

The release of FFAs from Pickering emulsions during simulated intestinal digestion is shown in Fig. 5C. During the first 30 minutes, FFAs were continuously released, followed by a plateau phase. After 2 hours of intestinal digestion, the pure WMG group, containing the highest amylopectin content, exhibited the highest FFAs release at 65.06 %. The FFAs release in the other groups was similar. Although there were slight differences in FFAs release among the other groups (ranging from 54.21% to 59.27%), these differences were not statistically significant (Fig. S5, Supplementary Materials). Notably, a strong negative correlation was observed between droplet size and FFA release (R^2 = 0.9994, Fig. S6), suggesting that the larger specific interfacial area of amylopectin-rich droplets promotes lipase adsorption and catalytic efficiency [55]. However, differences in lipolysis kinetics cannot be solely attributed to surface area effects. Instead, they are also governed by the intrinsic interfacial characteristics of the starch granules, as the more rigid and densely packed interfacial layer formed by high-amylose starch particles imposes an additional physical barrier that limits enzyme accessibility [56].

The rate of lipolysis during the intestinal phase is closely related to the potential applications of Pickering emulsions. For instance, emulsions with higher lipolysis efficiency during the intestinal phase can be used for delivering lipophilic active compounds or drugs [11]. Conversely, formulations that reduce lipolysis efficiency are more suitable as carriers for functional foods targeting obesity, diabetes, hyperlipidemia, and related metabolic disorders [57].

3.5. Digestive properties of Pickering emulsions stabilized by varying Amylose/Amylopectin ratios in the mouse digestive tract

Based on the *in vitro* simulated digestion results, the three groups with similar amylose/amylopectin ratios (HAMG/WMG ratios of 2:1, 1:1, and 1:2) showed no significant differences in particle size changes or FFAs release during digestion. Consequently, we selected three representative groups for *in vivo* studies using a mouse model: the HAMG group (HAMG/WMG = 1:0, 71.29% amylose and 28.71% amylopectin), the WMG group (HAMG/WMG = 0:1, 9.51% amylose and 90.49% amylopectin), and the HAMG/WMG group (HAMG/WMG = 1:1, 42.57 % amylose and 57.43 % amylopectin). Additionally, the control groups included a pure water group (CTRL) and a high-shear mixed sunflower seed oil-water group (SOW).

Following the administration of different Pickering emulsion formulations to mice, we analyzed the digestion status of emulsified lipids and measured TAGs and FFAs concentrations in various sections of the gastrointestinal tract. After 1 hour of digestion, significant amounts of oil droplets remained in the stomachs of all groups except the water group (Fig. 6A). The oil phase was more concentrated in the SOW and HAMG groups, while oil droplets in the WMG and HAMG/WMG groups were more dispersed. After 2 h, oil droplets were still observable in the stomachs of mice in the HAMG and HAMG/WMG groups, whereas only a few visible droplets remained in the SOW and WMG groups. This suggests that emulsions stabilized by HAMG and HAMG/WMG may influence lipid digestion kinetics, leading to changes in gastrointestinal hormones that in turn regulate a slower gastric emptying rate compared to those stabilized by SOW or WMG [58].

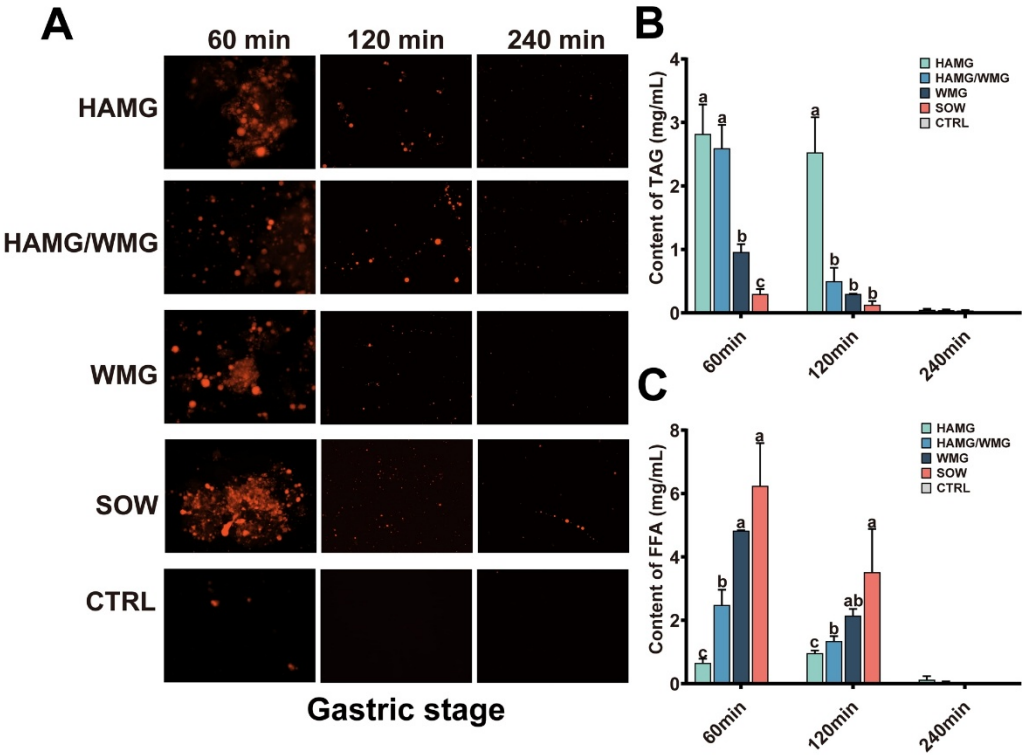

Fig. 6. (A) Fluorescence microscopy images of gastric contents collected at various time points after gavage with different Pickering emulsions. The oil phase was visualized by Nile Red staining. (B) Triacylglycerol (TAG) and (C) free fatty acid (FFA) contents in gastric digesta at the corresponding time points. Different letters indicate significant differences ($P < 0.05$).

One hour after gavage, during the small intestine digestion phase, the state of the oil droplets in the upper part of the small intestine in the HAMG group was similar to that observed in the stomach (Fig. 7A). In the other groups, the oil phase in the HAMG/WMG group was more concentrated, while the oil phase in the SOW

and WMG groups displayed a more dispersed distribution of oil droplets. With the extension of digestion time, the residual oil droplet content in the upper segment of the small intestine at 2 h and 4 h was minimal, existing as dispersed and individual droplets, with no significant differences among the groups. In the middle segment of the small intestine, only the HAMG group exhibited a considerable amount of oil droplets one hour after gavage (Fig. 8A). Based on observations from the stomach and the upper and middle segments of the small intestine, it can be demonstrated that emulsions stabilized by high-amylose maize starch granules (HAMG) effectively slow down lipid digestion and absorption, consistent with results from *in vitro* simulated digestion. The minimal lipid content observed in the samples from the lower segment of the small intestine at different digestion times suggests that most lipids were digested and absorbed before reaching this section (Fig. 9A).

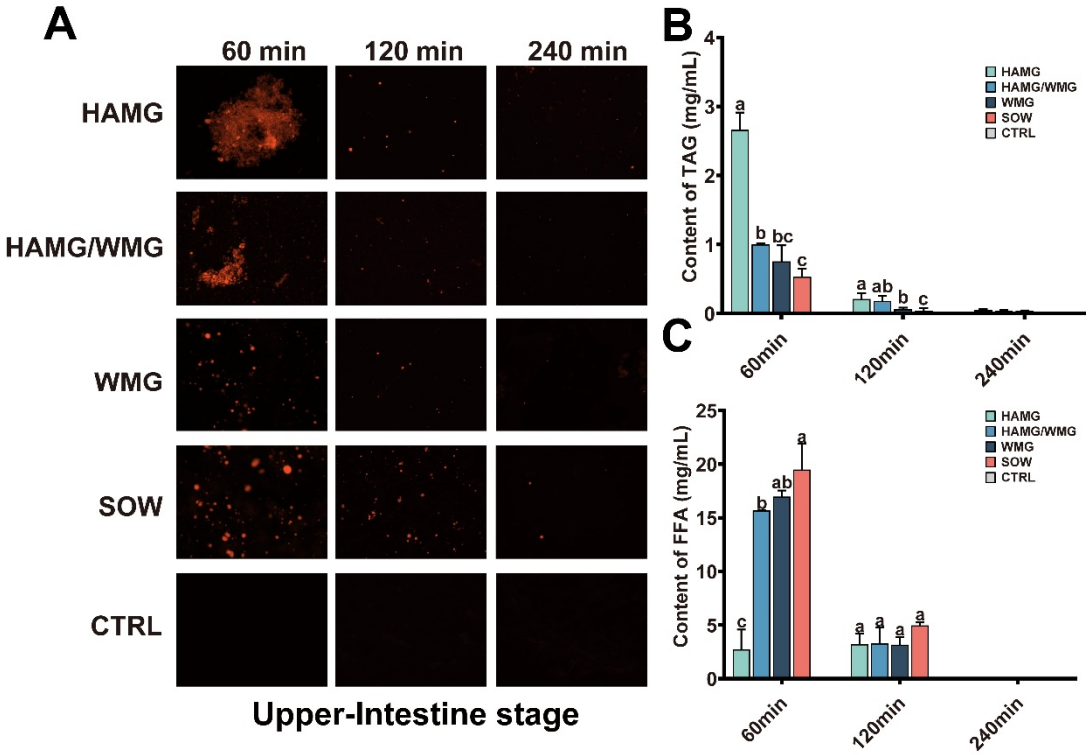

Fig. 7. (A) Fluorescence microscopy images of upper intestinal contents collected at various time points after gavage with different Pickering emulsions. The oil phase was visualized by Nile Red staining. (B) TAG and (C) FFA contents in upper intestinal digesta at the corresponding time points. Different letters indicate significant differences ($P < 0.05$).

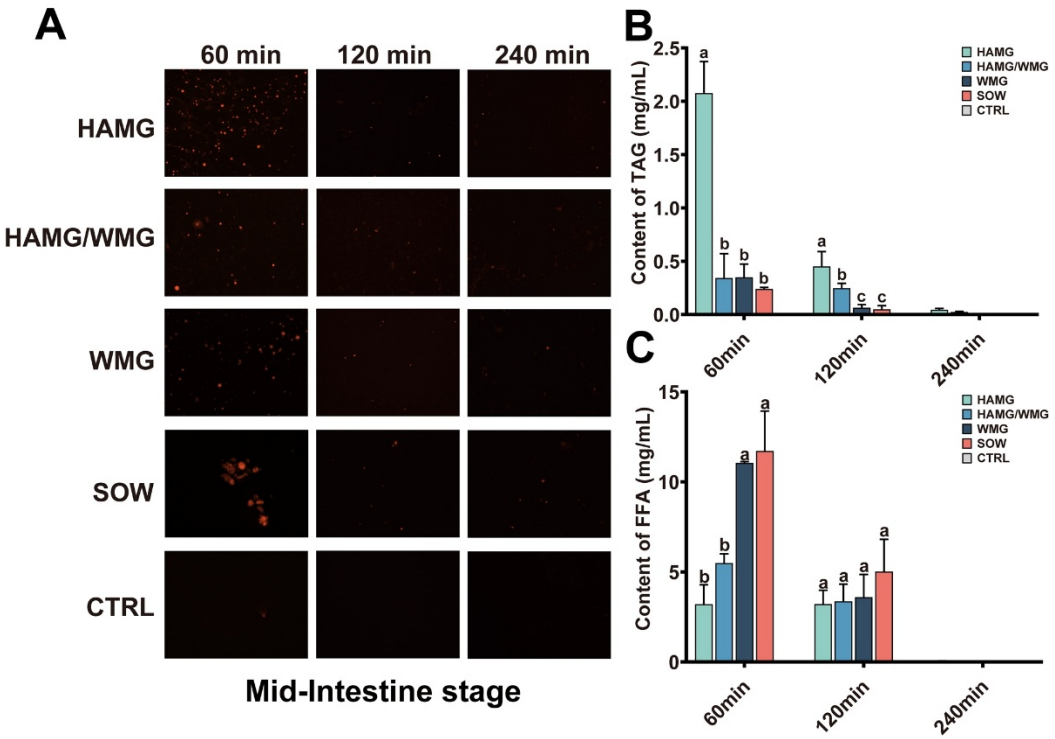

Fig. 8. (A) Fluorescence microscopy images of middle intestinal contents collected at various time points after gavage with different Pickering emulsions. The oil phase was visualized by Nile Red staining. (B) TAG and (C) FFA contents in middle intestinal digesta at the corresponding time points. Different letters indicate significant differences ($P < 0.05$).

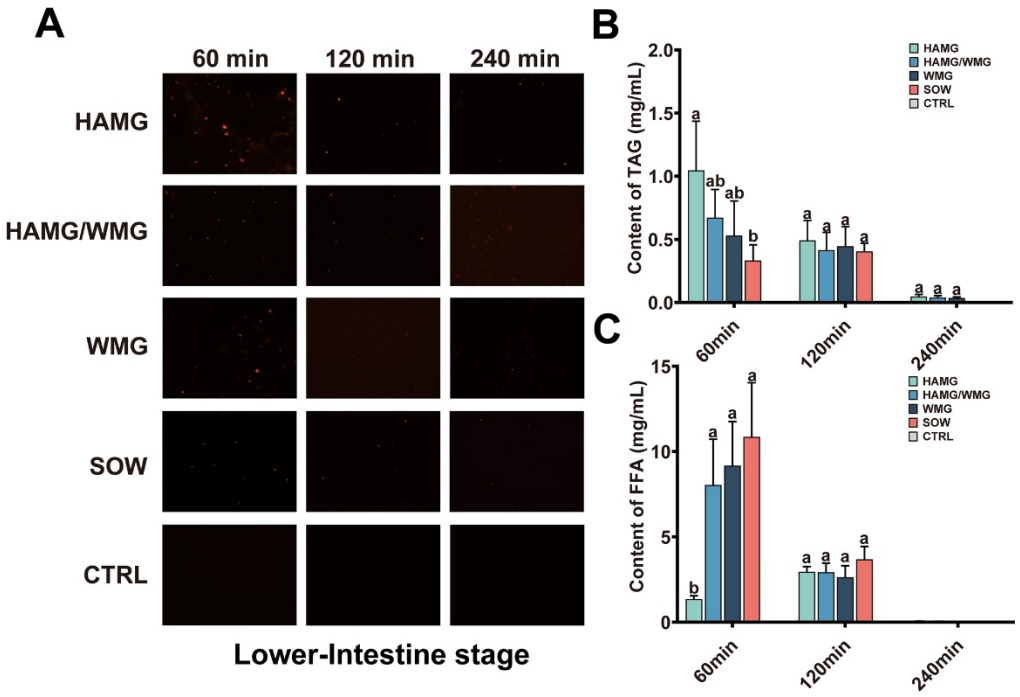

Fig. 9. (A) Fluorescence microscopy images of lower intestinal contents collected at various time points after gavage with different Pickering emulsions. The oil phase was visualized by Nile Red staining. (B) TAG and (C) FFA contents in lower intestinal digesta at the corresponding time points. Different letters indicate significant differences ($P < 0.05$).

The discrepancies in digestion behavior between *in vivo* and *in vitro* studies of chitosan-stabilized emulsions observed in previous research underscore the significance of *in vivo* studies for accurately understanding emulsion digestion [59, 60]. The results from tracking emulsion digestion in the mouse digestive tract align with those from *in vitro* simulated digestion, suggesting that the *in vivo* digestion behavior of Pickering emulsions, stabilized by varying amylose/amylopectin ratios, can be reliably predicted using *in*

vitro models. This consistency is in agreement with previous human studies showing that *in vitro*–predicted structural evolution and lipolysis kinetics closely reproduce *in vivo* digestive behavior [14, 61]. When considered alongside the findings of the present work, these results indicate that combining *in vitro* and *in vivo* experiments may provide more robust predictions of the digestive and physiological responses of Pickering emulsions in humans.

Despite the observed variations in gastric emptying rates and fat digestion at different stages, the prolonged transit time in the digestive tract resulted in minimal undigested fat residues in the lower small intestine across all emulsions. Thus, with sufficient digestion time, the overall extent of fat digestion is expected to exhibit minimal variation.

3.6. Effect of Pickering emulsions stabilized by varying Amylose/Amylopectin ratios on triglyceride and free fatty acids content in the mouse digestive tract

TAGs in emulsions are hydrolyzed by lipase in the digestive tract into FFAs, diglycerides, and monoglycerides [52]. This process occurs predominantly in the small intestine, with only a minor portion of lipid hydrolysis occurring in the stomach [62]. As illustrated in Fig. 6-9, the measured levels of TAGs and hydrolysis products, specifically FFAs, in the mouse digestive tract align with the digestive behavior of the emulsions observed under fluorescence microscopy.

During the gastric phase, TAG detection results indicated that all emulsions slowed gastric emptying of lipids compared to the simple oil-water mixture (SOW) (Fig. 6B). After 1 hour of gastric administration, the two high-amylose groups, HAMG and HAMG/WMG, exhibited the highest TAG levels, indicating a more effective delay in gastric emptying. Notably, in the HAMG group, gastric emptying was still effectively delayed even after 2 hours. However, after 4 hours of digestion, no lipid residues were detected in any of the treatment groups. Although the FFAs concentration in the stomach was relatively low compared to the small intestine phase, a clear trend emerged: higher amylose ratios corresponded to greater resistance to lipid degradation and FFAs production, consistent with *in vitro* simulated digestion results (Fig. 6C).

Consistent with the gastric phase, triglycerides and FFAs detection in small intestine contents showed that emulsions formed by high-amylose HAMG exhibited the most pronounced delay in lipid degradation, while emulsions formed by high-amylopectin WMG allowed for easier lipid digestion and absorption (Fig. 7B, 7C,8B,8C, 9B, and 9C). Although sampling and detection of gastrointestinal contents were challenging, and accuracy based on wet weight calculations could be affected, the observed trends remained consistent with *in vitro* simulated digestion results. Thus, higher amylose and lower amylopectin content in starch particles led to a stronger inhibitory effect of the resulting Pickering emulsions on lipid hydrolysis *in vivo*.

3.7. The effect of Pickering emulsions stabilized by different ratios of amylose/amylopectin on plasma triglyceride levels in mice

After lipid digestion and hydrolysis in the small intestine, the resulting digestive products are absorbed through the intestinal microvilli. These absorbed components are then re-esterified into TAGs in the

endoplasmic reticulum. The newly formed TAGs are assembled into chylomicrons and transported via the lymphatic system, eventually merging with the circulatory system [63].

Fig.10A depicts the changes in plasma total triglyceride (TG) levels in mice following gavage, relative to baseline values prior to gavage. One-hour post-gavage, there was no significant difference in the increase in TG levels between the emulsion groups and the SOW group; however, both were significantly higher than in the CTRL group, suggesting that dietary TAGs intake markedly elevates plasma TG levels. Two hours post-gavage, the TG levels in the SOW group were significantly higher than those in the emulsion groups, with no significant differences observed among the three emulsion groups. These findings suggest that, given equal total fat intake, Pickering emulsions may attenuate the postprandial rise in plasma TG levels. At three hours post-gavage, the TG levels among the emulsion groups began to diverge, with the HAMG group exhibiting significantly lower TG levels compared to the other emulsion groups—a trend that persisted at the four-hour time point. Despite a slight delay in the emergence of this trend, the results demonstrate an inverse relationship between plasma TG levels and TAGs concentrations in gastrointestinal contents, which align closely with the fluctuations in FFAs levels.

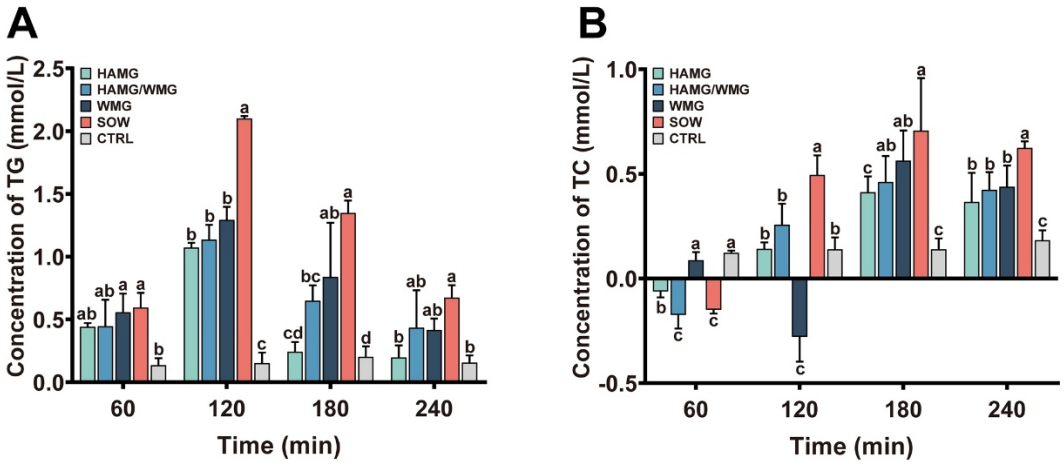

Fig. 10. Changes in (A) total triglyceride (TG) and (B) total cholesterol (TC) levels in mouse plasma at different time points after gavage with Pickering emulsions stabilized with varying amylose/amylopectin ratios. Different letters indicate significant differences ($P < 0.05$).

The consistency between *in vivo* experiments and *in vitro* simulated digestion has also been validated in human studies. Scheuble *et al.* demonstrated, by comparing *in vitro* digestion models with human MRI (Magnetic Resonance Imaging) measurements and plasma metabolite profiles, that gastric structuring and lipolysis kinetics observed *in vitro* can reliably predict *in vivo* digestive responses. Bertsch *et al.* further confirmed in human trials that the lipolysis-inhibiting effects of Pickering emulsions predicted from *in vitro* experiments were highly consistent with *in vivo* outcomes. Together with the present findings, these studies suggest that optimized *in vitro* digestion models, when combined with animal experiments, can provide a reliable framework for predicting human digestive and satiety responses to Pickering emulsions [14, 61].

Although the postprandial plasma total cholesterol (TC) levels in mice (Fig. 10B) exhibited a similar trend to TG levels at 3- and 4-hours post-gavage, the changes at 1 and 2 hours displayed distinct characteristics, differing markedly from the triglyceride trends. One-hour post-gavage, TC levels in the

HAMG, HAMG/WMG, and SOW groups were lower than their baseline levels. After 2 hours, the WMG group exhibited a further decline in TC levels, dropping below baseline. These findings suggest that, beyond dietary lipid intake, total plasma TC levels are influenced by additional factors, such as cholesterol synthesis and metabolism by organs like the liver. Consequently, the predictability of the effects of food emulsion interfaces on postprandial plasma TC levels remains limited, and the underlying causes and mechanisms warrant further detailed investigation.

Postprandial lipid metabolism is strongly linked to several diseases, especially cardiovascular diseases, diabetes, and obesity-related metabolic disorders [64-66]. Thus, controlling postprandial plasma lipid levels represents a crucial application area in functional food design [1]. Our findings indicate that Pickering emulsions, stabilized by varying amylose/amylopectin ratios, have potential as food matrices to mitigate postprandial lipid-associated diseases, offering a novel strategy for functional food development.

3.8. The effect of Pickering emulsions stabilized by different ratios of amylose/amylopectin on duodenum transcriptome

Animal experimental results demonstrate that Pickering emulsions stabilized by starch granules with differing amylose/amylopectin ratios exhibit distinct digestive behaviors throughout the digestive system. The current results showed that these divergences originate in the stomach and become amplified in the upper small intestine, where clear differences in emulsion integrity, lipid hydrolysis, and FFA accumulation were observed. Given the pivotal role of the duodenum as the primary site coordinating nutrient sensing, lipid absorption, and metabolic signaling, we therefore focused on this region to elucidate host transcriptional responses to emulsions with contrasting digestive behaviors. Accordingly, duodenal transcriptomes were analyzed one hour after gavage with Pickering emulsions stabilized by starch granules with extreme amylose/amylopectin ratios (HAMG and WMG).

By sequencing the transcriptomes of duodenal tissues, we obtained an average of 49.00±6.86, 49.33±3.56, and 48.97±4.34 million clean reads from the mice in the HAMG, WMG, and CTRL groups, respectively. The clean reads from each group were mapped to the mouse reference genome (http://asia.ensembl.org/Mus_musculus/Info/Index) with mapping rates of 96.64% for HAMG, 96.76% for WMG, and 96.61% for CTRL. Differentially expressed genes (DEGs) were identified by quantifying and comparing transcription levels of duodenal tissues among the groups.

As shown in Fig. 11A, only 16 genes were differentially expressed in the HAMG group compared with the CTRL group, with 4 genes upregulated and 12 downregulated, and the gene expression changes among individual mice across groups are presented in Fig. S7 (Supplementary Materials). This limited transcriptional response indicates that ingestion of HAMG-stabilized emulsions exerts only a minor impact on duodenal gene expression. Such transcriptional stability is consistent with previous observations of the unchanged state of the HAMG emulsion in the upper small intestine one hour after ingestion, along with the extremely low TAGs lipolysis efficiency and correspondingly low FFAs concentrations in the intestinal contents of HAMG-treated mice (Fig. 7B and 7C).

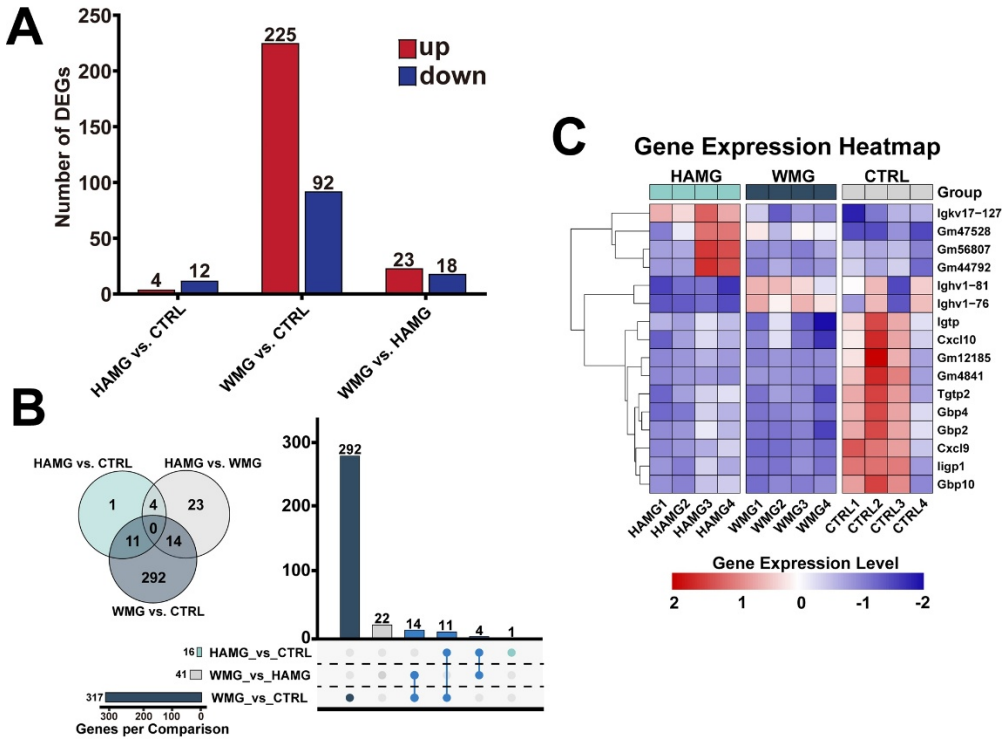

Fig. 11. (A) Significantly differentially expressed genes (DEGs) in duodenum tissues from different groups. (B) UpSet plot illustrating the intersection of DEGs across multiple comparisons. (C) Identified DEGs exhibited significant changes in expression levels in both the HAMG and WMG groups compared to the CTRL group. (D) Top enriched KEGG pathways in the WMG group compared to the CTRL group.

In contrast, the WMG group exhibited significant changes, with the expression of 317 genes in the duodenal transcriptome altered compared to the CTRL group, including 225 upregulated and 92 downregulated genes. The DEGs were enriched in several key pathways associated with energy metabolism and immune regulation, including oxidative phosphorylation, thermogenesis, and the NOD-like receptor signaling pathway (Fig. 11D). These enrichment results demonstrate that the rapid digestion of the WMG emulsion and the consequent nutrient surge in the duodenum comprehensively reprogrammed the local transcriptional landscape, driving adaptations in cellular energy production and immune surveillance. The wide-ranging variations are associated with the relative instability observed in the stomach and upper small intestine for WMG emulsions compared to HAMG emulsions. The higher concentration of lipids and metabolic by-products, as well as the metabolites produced from the degradation of amylopectin starch (WMG), significantly affected the nutritional microenvironment in the duodenum, leading to drastic fluctuations in the gene expression levels in this region.

Fig. 11B presents an UpSet plot illustrating the overlap of DEGs among experimental groups. Specifically, 11 genes were commonly altered in both the HAMG and WMG groups relative to the CTRL group. Fig. 11C provide a detailed representation of the transcriptional profiles of these 11 DEGs across experimental groups, emphasizing their regulatory dynamics in response to the treatments. Of these 11 genes, except for *Gm47582, Gm12185,* and *Gm4841*, which lack clear functional annotations, the remaining 8 genes—including *Igtp* (Immune-related Guanosine Triphosphatase M protein), *Cxcl10* (Interferon-γ-inducible protein 10), *Tgtp2* (Interferon-γ-induced GTPase), *Cxcl9* (Monokine induced by interferon-gamma), *Iigp1* (Interferon-gamma-inducible 47-kDa GTPase), *Gbp2* (Guanylate-binding protein

2), *Gbp4* (Guanylate-binding protein 4), and *Gbp10* (Guanylate-binding protein 10)—were significantly downregulated in both the WMG and HAMG groups compared to the CTRL group. These genes are classical interferon-stimulated genes involved in innate immune defense and are strongly induced by interferon signaling [67-69].

Previous studies have shown that fasting-induced energy stress markedly elevates interferon-γ expression across multiple tissues [70-72]. Accordingly, the coordinated downregulation of interferon-responsive genes observed here likely reflects a dynamic modulation of interferon signaling during the transition from fasting to postprandial states following emulsion ingestion.

3.9. WMG emulsion ingestion induces changes in the transcriptional levels of genes involved in lipid metabolism

To further elucidate the specific effects of WMG emulsion ingestion on duodenal function, the annotations of differentially expressed genes (compared to the CTRL group) were analyzed through the KEGG database to predict and interpret their functional and biological roles. According to Fig. 12A, KEGG database annotations suggest that DEGs are involved in various biological processes, including metabolism, cellular activities, organismal systems, and other related functions. Specifically, the top three functional categories are immune system, environmental adaptation, and energy metabolism. Enrichment analysis further indicated that environmental adaptation was predominantly associated with thermogenesis, with the genes involved overlapping substantially with those enriched in energy metabolism pathways, consistent with the KEGG pathway enrichment results shown in Fig. 11D.

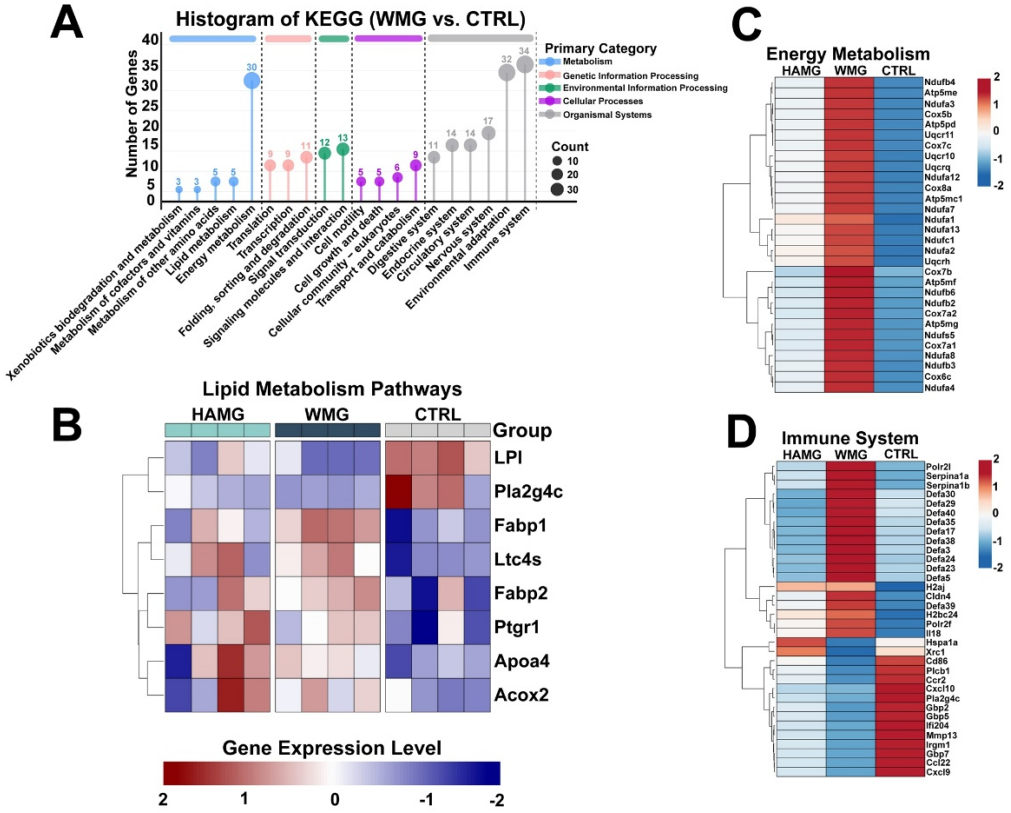

Fig. 12. (A) Annotation of DEGs (WMG vs. CTRL) in the KEGG database. (B) Relative expression levels of DEGs (WMG vs. CTRL) involved in lipid metabolism. Average relative expression levels of DEGs (WMG vs. CTRL) involved in (C) energy metabolism (oxidative phosphorylation) and (D) the immune system.

Given that structural modulation of emulsions aims to regulate lipid digestion and absorption, particular attention was paid to DEGs directly involved in intestinal lipid uptake, intracellular transport, and lipoprotein assembly (Fig. 12B). One hour after oral administration of the WMG emulsion, the relatively rapid hydrolysis of TAGs resulted in elevated levels of FFAs in the intestinal lumen. This increase was accompanied by a marked upregulation of *fabp1* and *fabp2*, which encode liver-type and intestinal-type fatty acid-binding proteins (FABPs), respectively [73]. FABPs play a pivotal role in facilitating intracellular trafficking of long-chain fatty acids across the enterocyte cytosol, thereby enhancing fatty acid absorption efficiency [74].

The elevated intracellular availability of FFAs and FABPs subsequently promoted chylomicron assembly, as evidenced by the significant upregulation of *Apoa4* transcription [75]. *ApoA4* is a key structural and regulatory component of chylomicrons and has been widely recognized as a sensitive marker of intestinal lipid absorption [76]. Enhanced *Apoa4* expression strongly suggests increased chylomicron formation and secretion, which facilitates the transport of dietary lipids through the lymphatic system into the systemic circulation [77]. This transcriptional response provides a molecular explanation for the significantly higher postprandial plasma TAG concentrations observed in the WMG group compared with the CTRL and HAMG groups.

In parallel, the transcriptional upregulation of *acox2*, encoding acyl-CoA oxidase 2 (ACOX2), indicates activation of peroxisomal β-oxidation pathways in response to increased FFA flux. ACOX2 catalyzes the initial and rate-limiting step in the peroxisomal oxidation of long-chain and branched-chain fatty acids, particularly those that are inefficiently processed by mitochondrial β-oxidation [78, 79]. The induction of *acox2* suggests an adaptive metabolic response aimed at preventing intracellular lipid overload by channeling excess fatty acids toward oxidative degradation [78, 80]. Consistent with this notion, genes involved in mitochondrial energy metabolism were also upregulated (Fig. 12C), indicating coordinated regulation between peroxisomal and mitochondrial fatty acid oxidation to accommodate increased lipid absorption.

Conversely, *lpl*, which encodes lipoprotein lipase responsible for hydrolyzing circulating TAGs into FFAs and glycerol, was significantly downregulated in the WMG group [81]. This suppression may reflect a negative feedback mechanism triggered by elevated intestinal and systemic FFA availability, thereby limiting further TAG hydrolysis and preventing excessive lipid accumulation. Additionally, *ltc4s* and *pla2g4c*, encoding leukotriene C4 synthase and cytosolic phospholipase A2 group IVC, respectively, were differentially expressed [82-84]. These genes serve as important molecular links between lipid metabolism and immune signaling, as they regulate the generation of lipid-derived inflammatory mediators. Their altered expression is consistent with the enrichment of immune system-related pathways (Fig. 11D), suggesting that enhanced lipid flux induced by WMG emulsion ingestion may concurrently modulate local immune responses in the duodenum.

3.10. WMG emulsion ingestion induces changes in the transcriptional levels of genes involved in duodenal energy metabolism and immune function

Compared to the CTRL group, the increased expression of lipid metabolism-related genes *acox2, ltc4s,* and *plag4c* in the WMG group suggests that alterations in lipid metabolism may lead to changes in energy metabolism and immune response. Notably, these transcriptional changes are consistent with the markedly elevated luminal FFA levels observed in the upper small intestine following WMG emulsion ingestion, suggesting that increased lipid flux acts as a primary metabolic stimulus in the duodenum.

KEGG enrichment analysis further revealed that 30 differentially expressed genes associated with energy metabolism were significantly enriched in the WMG group (Fig. 12C), with all of these genes being upregulated and predominantly involved in mitochondrial oxidative phosphorylation. Specifically, genes encoding multiple subunits of mitochondrial complex I (NADH: coenzyme Q reductase), including *ndufa1, ndufa2, ndufa3, ndufa4, ndufa7, ndufa8, ndufa12, ndufa13, ndufb2, ndufb3, ndufb4,* and *ndufs5,* were significantly increased [85]. In parallel, genes encoding ATP synthase (complex V) subunits, such as *atp5me, atp5mg, atp5mf, atp5pd,* and *atp5mc1,* were also upregulated, indicating enhanced ATP synthesis capacity [86]. Additionally, transcriptional activation of genes encoding components of the mitochondrial cytochrome bc1 complex (*uqcrh, uqcr10, uqcr11,* and *uqcrq*) and cytochrome c oxidase (*cox7a1, cox7a2, cox5b, cox6c, cox7c,* and *cox8a*) further supports a global elevation of mitochondrial respiratory activity [87, 88]. Functionally, the coordinated upregulation of oxidative phosphorylation–related genes is indicative of enhanced mitochondrial oxidative capacity in response to the elevated fatty acid availability following rapid TAG hydrolysis in the WMG group. This transcriptional shift is consistent with the well-documented oscillatory responses of mitochondrial metabolism during fasting–refeeding transitions, in which abrupt changes in nutrient flux rapidly remodel mitochondrial activity in intestinal epithelial cells [89].

Research on fasting-refeeding has shown that nutritional signals are critical in maintaining intestinal immune homeostasis [90]. The increase in mitochondrial oxidative phosphorylation is likely to trigger a cascade of effects, such as the production of reactive oxygen species (ROS) [91], immune cell dynamics, and mucosal immune responses [90], potentially resulting in more significant biological effects. In line with this concept, genes encoding α-defensins (*defa3, defa5, defa17, defa23, defa24, defa29, defa30, defa35, defa38, defa39,* and *defa40*) were markedly upregulated in the duodenum of mice administered WMG emulsions compared with CTRL mice (Fig. 12D). α-Defensins are key antimicrobial peptides secreted by Paneth cells and play critical roles in shaping the intestinal microbial ecosystem and maintaining mucosal immune defense[92].

Conversely, several interferon-stimulated genes, including *cxcl9, cxcl10, gbp2, gbp5, gbp7, lif204,* and *irgm1*, were downregulated in the WMG group. This transcriptional suppression likely reflects dynamic modulation of IFN-γ–dependent immune signaling during the transition from fasting to postprandial states, as nutritional cues are known to inversely regulate interferon responses during fasting–refeeding cycles [93, 94]. Collectively, these results demonstrate that rational emulsion design alters lipid digestion kinetics, thereby reshaping the duodenal nutrient microenvironment and coordinately regulating mitochondrial metabolism and immune-related gene networks.

4. Conclusion

In this study, the properties of Pickering emulsions stabilized by starch granules with varying amylose/amylopectin ratios were analyzed, along with their digestive behavior in both *in vitro* and *in vivo* models. Additionally, their effects on blood lipid levels and the transcriptome profiles of small intestine (duodenum) tissues were assessed using a mouse model. The results indicate that the amylose and amylopectin content play a critical role in determining particle size and emulsion digestibility. Emulsions stabilized by high-amylose HAMG were more stable and resistant to digestion in both *in vitro* and *in vivo* systems, as evidenced by slower lipid hydrolysis and absorption. In contrast, emulsions stabilized by high-amylopectin WMG exhibited faster lipid digestion and higher release of FFAs in the small intestine, potentially due to the more accessible branched structure of amylopectin. These findings, combined with blood lipid level measurements in the mouse model, demonstrate that Pickering emulsions stabilized by starch granules with different amylose-to-amylopectin ratios can regulate lipid absorption and transport.

Transcriptome analysis of the duodenum revealed significant differences between the HAMG and WMG groups, with WMG inducing the upregulation of several genes involved in lipid metabolism, immune response, and mitochondrial oxidative phosphorylation. In contrast, the HAMG group exhibited minimal changes in gene expression, suggesting a more stable metabolic response. These findings highlight the role of starch structure in modulating digestive and metabolic processes, indicating that emulsions formulated with specific amylose-to-amylopectin ratios can be used to regulate nutrient release, lipid digestion and absorption, and reprogram metabolic and immune responses in the digestive tract. Furthermore, while the *in vitro* digestion model is useful, it may not fully reflect the complexities of *in vivo* digestion. Although the results from the mouse model cannot be directly extrapolated to humans, this model provided valuable insights into lipid metabolism and immune-related gene expression. Overall, this study establishes a promising foundation for the development of food matrix designs that aim to regulate metabolism and immune function through targeted nutrient delivery systems.

This study has several limitations that require clarification and indicate directions for future research. First, in terms of experimental methodology, the preparation of the Pickering emulsions was subject to constraints in parameter control due to equipment limitations. Future work should employ more standardized preparation protocols to establish a controllable and reproducible experimental system. More importantly, the study design has a critical limitation: although the emulsion formulation was deliberately simplified to include only starch and lipids as basic nutrients, the analysis of the effects of emulsion structure on lipid metabolism and the duodenal transcriptome considered only differences in lipid release caused by physical structural disruption. The potential confounding effects of starch digestion and metabolism on duodenal function were not fully assessed. Further research is therefore needed to elucidate the impact of starch digestion and metabolism on the duodenum. Precisely designed emulsions or other food systems enabling targeted nutrient release within the gastrointestinal tract hold substantial promise for applications in medical nutrition.

Declaration of competing interest

The authors declared that they have no conflicts of interest to this work.

Acknowledgements

This study was supported by the Central Guidance Special Funds for Local Science and Technology Development (YDZX2024037), and Science and Technology Plan Project of Yunnan Province (202101BD070001-092).

Reference

1. McClements, D.J., E.A. Decker and Y. Park, Controlling lipid bioavailability through physicochemical and structural approaches. Crit Rev Food Sci Nutr, 2009. **49**(1): p. 48-67. https://doi.org/10.1080/10408390701764245
2. Jin, Y., P.J. Wilde, Y. Hou, et al., An evolving view on food viscosity regulating gastric emptying. Crit Rev Food Sci Nutr, 2023. **63**(22): p. 5783-5799. https://doi.org/10.1080/10408398.2021.2024132
3. Singh, H., A. Ye and D. Horne, Structuring food emulsions in the gastrointestinal tract to modify lipid digestion. Prog Lipid Res, 2009. **48**(2): p. 92-100. https://doi.org/10.1016/j.plipres.2008.12.001
4. Petrenko, V., F. Sinturel, H. Riezman, et al., Lipid metabolism around the body clocks. Prog Lipid Res, 2023. **91**: p. 101235. https://doi.org/10.1016/j.plipres.2023.101235
5. Zechner, R., R. Zimmermann, T.O. Eichmann, et al., Fat signals-lipases and lipolysis in lipid metabolism and signaling. Cell Metab, 2012. **15**(3): p. 279-291. https://doi.org/10.1016/j.cmet.2011.12.018
6. Maxfield, F.R. and I. Tabas, Role of cholesterol and lipid organization in disease. Nature, 2005. **438**(7068): p. 612-621. https://doi.org/10.1038/nature04399
7. Ko, C.W., J. Qu, D.D. Black, et al., Regulation of intestinal lipid metabolism: current concepts and relevance to disease. Nat Rev Gastro Hepat, 2020. **17**(3): p. 169-183. https://doi.org/10.1038/s41575-019-0250-7
8. Duca, F.A., T.M.Z. Waise, W.T. Peppler, et al., The metabolic impact of small intestinal nutrient sensing. Nat Commun., 2021. **12**(1): p. 903. https://doi.org/10.1038/s41467-021-21235-y
9. Qiu, J., Y. Ma and J. Qiu, Regulation of intestinal immunity by dietary fatty acids. Mucosal Immunol, 2022. **15**(5): p. 846-856. https://doi.org/10.1038/s41385-022-00547-2
10. Wymann, M.P. and R. Schneiter, Lipid signalling in disease. Nat Rev Mol Cell Biol, 2008. **9**(2): p. 162-176. https://doi.org/10.1038/nrm2335
11. McClements, D.J., E.A. Decker, Y. Park, et al., Structural design principles for delivery of bioactive components in nutraceuticals and functional foods. Crit Rev Food Sci Nutr, 2009. **49**(6): p. 577-606. https://doi.org/10.1080/10408390902841529
12. Torres, O., B.S. Murray and A. Sarkar, Overcoming in vitro gastric destabilisation of emulsion droplets using emulsion microgel particles for targeted intestinal release of fatty acids. Food Hydrocoll, 2019. **89**: p. 523-533. https://doi.org/10.1016/j.foodhyd.2018.11.010
13. Salvia-Trujillo, L., S.H.E. Verkempinck, L. Sun, et al., Lipid digestion, micelle formation and carotenoid bioaccessibility kinetics: Influence of emulsion droplet size. Food Chem, 2017. **229**: p. 653-662. https://doi.org/10.1016/j.foodchem.2017.02.146
14. Scheuble, N., J. Schaffner, M. Schumacher, et al., Tailoring emulsions for controlled lipid release: establishing in vitro–in vivo correlation for digestion of lipids. ACS Appl Mater Interfaces, 2018. **10**(21): p. 17571-17581. https://doi.org/10.1021/acsami.8b02637
15. Iqbal, S., P. Zhang, P. Wu, et al., Modulation of viscosity, microstructure and lipolysis of W/O emulsions by cellulose ethers during in vitro digestion in the dynamic and semi-dynamic gastrointestinal models. Food Hydrocoll, 2022. **128**: p. 107584. https://doi.org/10.1016/j.foodhyd.2022.107584
16. McClements, D.J. and C.E. Gumus, Natural emulsifiers - Biosurfactants, phospholipids, biopolymers, and colloidal particles: Molecular and physicochemical basis of functional performance. Adv Colloid Interface Sci, 2016. **234**: p. 3-26. https://doi.org/10.1016/j.cis.2016.03.002

17. Chassaing, B., T. Van de Wiele, J. De Bodt, et al., Dietary emulsifiers directly alter human microbiota composition and gene expression ex vivo potentiating intestinal inflammation. Gut, 2017. **66**(8): p. 1414-1427. https://doi.org/10.1136/gutjnl-2016-313099
18. Niroula, A., T.D. Gamot, C.W. Ooi, et al., Biomolecule-based pickering food emulsions: Intrinsic components of food matrix, recent trends and prospects. Food Hydrocoll, 2021. **112**: p. 106303. https://doi.org/10.1016/j.foodhyd.2020.106303
19. Ge, S., L. Xiong, M. Li, et al., Characterizations of Pickering emulsions stabilized by starch nanoparticles: Influence of starch variety and particle size. Food Chem, 2017. **234**: p. 339-347. https://doi.org/10.1016/j.foodchem.2017.04.150
20. Li, C., Y. Li, P. Sun, et al., Pickering emulsions stabilized by native starch granules. Colloids Surfaces A, 2013. **431**: p. 142-149. https://doi.org/10.1016/j.colsurfa.2013.04.025
21. Shi, Y.-C. and P.A. Seib, The structure of four waxy starches related to gelatinization and retrogradation. Carbohydr Res, 1992. **227**: p. 131-145. https://doi.org/10.1016/0008-6215(92)85066-9
22. Tester, R.F., J. Karkalas and X. Qi, Starch—composition, fine structure and architecture. J Cereal Sci, 2004. **39**(2): p. 151-165. https://doi.org/10.1016/j.jcs.2003.12.001
23. Liu, H., L. Wang, R. Cao, et al., In vitro digestibility and changes in physicochemical and structural properties of common buckwheat starch affected by high hydrostatic pressure. Carbohydr Polym, 2016. **144**: p. 1-8. https://doi.org/10.1016/j.carbpol.2016.02.028
24. Zhu, F., Starch based Pickering emulsions: Fabrication, properties, and applications. Trends Food Sci Technol, 2019. **85**: p. 129-137. https://doi.org/10.1016/j.tifs.2019.01.012
25. Shabir, I., A.H. Dar, K.K. Dash, et al., Formulation, characterization, and applications of organic Pickering emulsions: A comprehensive review. J Agr Food Res, 2023. **14**: p. 100853. https://doi.org/10.1016/j.jafr.2023.100853
26. Bai, Y., Y. Zhou, R. Zhang, et al., Gut microbial fermentation promotes the intestinal anti-inflammatory activity of Chinese yam polysaccharides. Food Chem, 2023. **402**: p. 134003. https://doi.org/10.1016/j.foodchem.2022.134003
27. Lu, X., Y. Wang, Y. Li, et al., Assembly of Pickering emulsions using milled starch particles with different amylose/amylopectin ratios. Food Hydrocoll, 2018. **84**: p. 47-57. https://doi.org/10.1016/j.foodhyd.2018.05.045
28. Ke, Q., X. Gong, S. Liao, et al., Effects of thermostats/barostats on physical properties of liquids by molecular dynamics simulations. J Mol Liq, 2022. **365**: p. 120116. https://doi.org/10.1016/j.molliq.2022.120116
29. Brodkorb, A., L. Egger, M. Alminger, et al., INFOGEST static in vitro simulation of gastrointestinal food digestion. Nat Protoc, 2019. **14**(4): p. 991-1014. https://doi.org/10.1038/s41596-018-0119-1
30. Marefati, A., B. Wiege, N. Abdul Hadi, et al., In vitro intestinal lipolysis of emulsions based on starch granule Pickering stabilization. Food Hydrocoll, 2019. **95**: p. 468-475. https://doi.org/10.1016/j.foodhyd.2019.04.051
31. Benito-Gallo, P., A. Franceschetto, J.C.M. Wong, et al., Chain length affects pancreatic lipase activity and the extent and pH–time profile of triglyceride lipolysis. Eur J Pharm Biopharm, 2015. **93**: p. 353-362. https://doi.org/10.1016/j.ejpb.2015.04.027
32. Chatzidaki, M.D., E. Mateos-Diaz, F. Leal-Calderon, et al., Water-in-oil microemulsions versus emulsions as carriers of hydroxytyrosol: an in vitro gastrointestinal lipolysis study using the pHstat technique. Food Funct, 2016. **7**(5): p. 2258-2269. https://doi.org/10.1039/C6FO00361C
33. Nikbakht Nasrabadi, M., A. Sedaghat Doost, S.A.H. Goli, et al., Effect of thymol and Pickering stabilization on in-vitro digestion fate and oxidation stability of plant-derived flaxseed oil emulsions. Food Chem, 2020. **311**: p. 125872. https://doi.org/10.1016/j.foodchem.2019.125872
34. Demopoulos, C.A., N.K. Andrikopoulos and S. Antonopoulou, A simple and precise method for the routine determination of platelet-activating factor in blood and urine. Lipids, 1994. **29**: p. 305-309. https://doi.org/10.1007/BF02536336
35. Folch, J., M. Lees and G.H. Sloane Stanley, A simple method for the isolation and purification of total lipides from animal tissues. J Biol Chem, 1957. **226**(1): p. 497-509. https://doi.org/10.1016/S0021-9258(18)64849-5
36. Li, B. and C.N. Dewey, RSEM: accurate transcript quantification from RNA-Seq data with or without a reference genome. Bioinformatics, 2011. **12**: p. 323. https://doi.org/10.1186/1471-2105-12-323
37. Love, M.I., W. Huber and S. Anders, Moderated estimation of fold change and dispersion for RNA-seq data with DESeq2. Genome Biol Evol, 2014. **15**(12): p. 550. https://doi.org/10.1186/s13059-014-0550-8

38. Wang, L., Z. Feng, X. Wang, et al., DEGseq: an R package for identifying differentially expressed genes from RNA-seq data. Bioinformatics, 2010. **26**(1): p. 136-138. https://doi.org/10.1093/bioinformatics/btp612
39. Xie, C., X. Mao, J. Huang, et al., KOBAS 2.0: a web server for annotation and identification of enriched pathways and diseases. Nucleic Acids Res, 2011. **39**: p. W316-22. https://doi.org/10.1093/nar/gkr483
40. Salimi, M., B.E. Channab, A. El Idrissi, et al., A comprehensive review on starch: Structure, modification, and applications in slow/controlled-release fertilizers in agriculture. Carbohydr Polym, 2023. **322**: p. 121326. https://doi.org/10.1016/j.carbpol.2023.121326
41. Zhu, M., W. Xiong, L. Devkota, et al., Ultrasound-induced changes in the structure and functionality of starch and protein. Food Hydrocoll, 2026. **172**: p. 112111. https://doi.org/10.1016/j.foodhyd.2025.112111
42. Song, X., Y. Pei, M. Qiao, et al., Preparation and characterizations of Pickering emulsions stabilized by hydrophobic starch particles. Food Hydrocoll, 2015. **45**: p. 256-263. https://doi.org/10.1016/j.foodhyd.2014.12.007
43. Saari, H., M. Rayner and M. Wahlgren, Effects of starch granules differing in size and morphology from different botanical sources and their mixtures on the characteristics of Pickering emulsions. Food Hydrocoll, 2019. **89**: p. 844-855. https://doi.org/10.1016/j.foodhyd.2018.11.063
44. Rayner, M., A. Timgren, M. Sjöö, et al., Quinoa starch granules: A candidate for stabilising food-grade Pickering emulsions. J Sci Food Agric, 2012. **92**: p. 1841-7. https://doi.org/10.1002/jsfa.5610
45. Li, J., Q. Wang, F. Meng, et al., Analysis of instability of starch-based Pickering emulsion under acidic condition of pH < 4 and improvement of emulsion stability. Int J Biol Macromol, 2024. **261**: p. 129886. https://doi.org/10.1016/j.ijbiomac.2024.129886
46. Saari, H., K. Heravifar, M. Rayner, et al., Preparation and Characterization of Starch Particles for Use in Pickering Emulsions. Cereal Chem, 2016. **93**(2): p. 116-124. https://doi.org/10.1094/CCHEM-05-15-0107-R
47. Dickinson, E., Use of nanoparticles and microparticles in the formation and stabilization of food emulsions. Trends Food Sci Technol, 2012. **24**(1): p. 4-12. https://doi.org/10.1016/j.tifs.2011.09.006
48. Binks, B.P., Particles as surfactants—similarities and differences. Curr Opin Colloid Interface Sci, 2002. **7**(1): p. 21-41. https://doi.org/10.1016/S1359-0294(02)00008-0
49. Clements, D., Food Emulsions : principles, practices and techniques. 2005.
50. Hou, Y., P. Shen, R. Wang, et al., Mechanism of fat globule size and surface composition regulating in vitro dynamic digestion, absorption and transport of structured emulsions. Food Hydrocoll, 2023. **142**: p. 108785. https://doi.org/10.1016/j.foodhyd.2023.108785
51. Junejo, S.A., B.M. Flanagan, B. Zhang, et al., Starch structure and nutritional functionality - Past revelations and future prospects. Carbohydr Polym, 2022. **277**: p. 118837. https://doi.org/10.1016/j.carbpol.2021.118837
52. Acevedo-Fani, A. and H. Singh, Biophysical insights into modulating lipid digestion in food emulsions. Prog. Lipid Res., 2022. **85**: p. 101129. https://doi.org/https://doi.org/10.1016/j.plipres.2021.101129
53. Tian, Y., B.L. Petersen, X. Liu, et al., Characterization of different high amylose starch granules. Part II: Structure evolution during digestion and distinct digestion mechanisms. Food Hydrocoll, 2024. **149**: p. 109593. https://doi.org/10.1016/j.foodhyd.2023.109593
54. Zhu, C., M. Zhang, A. Yang, et al., Thermal stability and in vitro digestive behavior of Pickering emulsion stabilized by high-amylose starch nanocrystals. Int J Biol Macromol, 2024. **280**: p. 136110. https://doi.org/10.1016/j.ijbiomac.2024.136110
55. Seimon, R.V., T. Wooster, B. Otto, et al., The droplet size of intraduodenal fat emulsions influences antropyloroduodenal motility, hormone release, and appetite in healthy males2. Am J Clin Nutr 2009. **89**(6): p. 1729-1736. https://doi.org/10.3945/ajcn.2009.27518
56. McClements, D.J. and Y. Li, Structured emulsion-based delivery systems: Controlling the digestion and release of lipophilic food components. Adv Colloid Interface Sci, 2010. **159**(2): p. 213-228. https://doi.org/10.1016/j.cis.2010.06.010
57. Li, J., H. Duan, Y. Liu, et al., Biomaterial-based therapeutic strategies for obesity and its comorbidities. Pharmaceutics, 2022. **14**(7): p. 1445. https://doi.org/10.3390/pharmaceutics14071445
58. Moran, T.H. and K.P. Kinzig, Gastrointestinal satiety signals II. Cholecystokinin. Am J Physiol-Gaster L, 2004. **286**(2): p. G183-G188. https://doi.org/abs/10.1152/ajpgi.00434.2003

59. Labourdenne, S., O. Brass, M. Ivanova, et al., Effects of colipase and bile salts on the catalytic activity of human pancreatic lipase. A study using the oil drop tensiometer. Biochemistry, 1997. **36**(12): p. 3423-3429. https://doi.org/10.1021/bi961331k
60. Park, G.Y., S. Mun, Y. Park, et al., Influence of encapsulation of emulsified lipids with chitosan on their in vivo digestibility. Food Chem, 2007. **104**(2): p. 761-767. https://doi.org/10.1016/j.foodchem.2006.12.020
61. Bertsch, P., A. Steingoetter, M. Arnold, et al., Lipid emulsion interfacial design modulates human in vivo digestion and satiation hormone response. Food Funct, 2022. **13**(17): p. 9010-9020. https://doi.org/10.1039/d2fo01247b
62. Iqbal, J. and M.M. Hussain, Intestinal lipid absorption. Am J Physiol-Endoc M, 2009. **296**(6): p. E1183-E1194. https://doi.org/10.1152/ajpendo.90899.2008
63. Hussain, M.M., Intestinal lipid absorption and lipoprotein formation. Curr Opin Lipidol, 2014. **25**(3): p. 200-206. https://doi.org/10.1097/mol.0000000000000084
64. Nakamura, A., Y. Monma, S. Kajitani, et al., Different postprandial lipid metabolism and insulin resistance between non-diabetic patients with and without coronary artery disease. J Cardiol, 2015. **66**(5): p. 435-444. https://doi.org/10.1016/j.jjcc.2015.02.005
65. López-Miranda, J., P. Pérez-Martínez, C. Marín, et al., Postprandial lipoprotein metabolism, genes and risk of cardiovascular disease. Curr Opin Lipidol, 2006. **17**(2): p. 132-138. https://doi.org/10.1097/01.mol.0000217894.85370.c2
66. Martins, I.J. and T.G. Redgrave, Obesity and post-prandial lipid metabolism. Feast or famine? J Nutr Biochem, 2004. **15**(3): p. 130-141. https://doi.org/10.1016/j.jnutbio.2003.10.006
67. Kim, B.H., J.D. Chee, C.J. Bradfield, et al., Interferon-induced guanylate-binding proteins in inflammasome activation and host defense. Nat Immunol, 2016. **17**(5): p. 481-489. https://doi.org/10.1038/ni.3440
68. Tokunaga, R., W. Zhang, M. Naseem, et al., CXCL9, CXCL10, CXCL11/CXCR3 axis for immune activation - A target for novel cancer therapy. Cancer Treat Rev, 2018. **63**: p. 40-47. https://doi.org/10.1016/j.ctrv.2017.11.007
69. Uthaiah, R.C., G.J. Praefcke, J.C. Howard, et al., IIGP1, an interferon-gamma-inducible 47-kDa GTPase of the mouse, showing cooperative enzymatic activity and GTP-dependent multimerization. J Biol Chem, 2003. **278**(31): p. 29336-29343. https://doi.org/10.1074/jbc.M211973200
70. Lee, J., S.J. Kim, T.G. Son, et al., Interferon-gamma is up-regulated in the hippocampus in response to intermittent fasting and protects hippocampal neurons against excitotoxicity. J Neurosci Res, 2006. **83**(8): p. 1552-1557. https://doi.org/10.1002/jnr.20831
71. Harney, D.J., M. Cielesh, G.E. Roberts, et al., Dietary restriction induces a sexually dimorphic type I interferon response in mice with gene-environment interactions. Cell Reports, 2023. **42**(6): p. 112559. https://doi.org/10.1016/j.celrep.2023.112559
72. Mallu, A.C.T., M. Vasudevan, S. Allanki, et al., Prediabetes uncovers differential gene expression at fasting and in response to oral glucose load in immune cells. Clin Nutr, 2021. **40**(3): p. 1247-1259. https://doi.org/10.1016/j.clnu.2020.08.007
73. Storch, J. and A.E. Thumser, Tissue-specific functions in the fatty acid-binding protein family. J Biol Chem, 2010. **285**(43): p. 32679-32683. https://doi.org/10.1074/jbc.R110.135210
74. Pickens, C.A., L.M. Sordillo, S.S. Comstock, et al., Plasma phospholipids, non-esterified plasma polyunsaturated fatty acids and oxylipids are associated with BMI. Prostag Leukotr Ess, 2015. **95**: p. 31-40. https://doi.org/10.1016/j.plefa.2014.12.001
75. Neeli, I., S.A. Siddiqi, S. Siddiqi, et al., Liver fatty acid-binding protein initiates budding of pre-chylomicron transport vesicles from intestinal endoplasmic reticulum. J Biol Chem, 2007. **282**(25): p. 17974-17984. https://doi.org/10.1074/jbc.M610765200
76. Tso, P., W. Sun and M. Liu, Gastrointestinal satiety signals IV. Apolipoprotein A-IV. Am J Physiol-Gaster L, 2004. **286**(6): p. G885-90. https://doi.org/10.1152/ajpgi.00511.2003
77. Borén, J., M.R. Taskinen, E. Björnson, et al., Metabolism of triglyceride-rich lipoproteins in health and dyslipidaemia. Nat Rev Cardiol, 2022. **19**(9): p. 577-592. https://doi.org/10.1038/s41569-022-00676-y
78. Waterham, H.R., S. Ferdinandusse and R.J. Wanders, Human disorders of peroxisome metabolism and biogenesis. Antioxid Redox Signal, 2016. **1863**(5): p. 922-933. https://doi.org/10.1016/j.bbamcr.2015.11.015
79. Perez, D.H., A. Mondal, W. Xu, et al., ATP allosterically regulates an acyl-CoA oxidase. Nat Commun, 2025. **16**(1): p. 7318. https://doi.org/10.1038/s41467-025-61905-9
80. Zhang, Y., Y. Chen, Z. Zhang, et al., Acox2 is a regulator of lysine crotonylation that mediates hepatic metabolic homeostasis in mice. Cell Death Dis, 2022. **13**(3): p. 279. https://doi.org/10.1038/s41419-022-04725-9

81. Azeez, O.I., R. Meintjes and J.P. Chamunorwa, Fat body, fat pad and adipose tissues in invertebrates and vertebrates: the nexus. Lipids Health Dis, 2014. **13**: p. 71. https://doi.org/10.1186/1476-511x-13-71
82. Lam, B.K. and K.F. Austen, Leukotriene C4 synthase: a pivotal enzyme in cellular biosynthesis of the cysteinyl leukotrienes. Prostag Oth Lipid M, 2002. **68-69**: p. 511-520. https://doi.org/10.1016/s0090-6980(02)00052-7
83. Fujimori, K., S. Uno, K. Kuroda, et al., Leukotriene C(4) synthase is a novel PPARγ target gene, and leukotriene C(4) and D(4) activate adipogenesis through cysteinyl LT1 receptors in adipocytes. Bba-mol Cell Res, 2022. **1869**(3): p. 119203. https://doi.org/10.1016/j.bbamcr.2021.119203
84. Ghosh, M., D.E. Tucker, S.A. Burchett, et al., Properties of the Group IV phospholipase A2 family. Prog Lipid Res, 2006. **45**(6): p. 487-510. https://doi.org/10.1016/j.plipres.2006.05.003
85. Okoye, C.N., S.A. Koren and A.P. Wojtovich, Mitochondrial complex I ROS production and redox signaling in hypoxia. Redox Biol, 2023. **67**: p. 102926. https://doi.org/10.1016/j.redox.2023.102926
86. Jonckheere, A.I., J.A. Smeitink and R.J. Rodenburg, Mitochondrial ATP synthase: architecture, function and pathology. Inherit Metab Dis, 2012. **35**(2): p. 211-225. https://doi.org/10.1007/s10545-011-9382-9
87. Teintze, M., M. Slaughter, H. Weiss, et al., Biogenesis of mitochondrial ubiquinol:cytochrome c reductase (cytochrome bc1 complex). Precursor proteins and their transfer into mitochondria. J Biol Chem, 1982. **257**(17): p. 10364-10371. https://doi.org/10.1016/S0021-9258(18)34028-6
88. Čunátová, K., D.P. Reguera, J. Houštěk, et al., Role of cytochrome c oxidase nuclear-encoded subunits in health and disease. Prog Lipid Res, 2020. **69**(6): p. 947-965. https://doi.org/10.33549/physiolres.934446
89. Ripa, R., E. Ballhysa, J.D. Steiner, et al., Refeeding-associated $AMPK_{\gamma 1}$ complex activity is a hallmark of health and longevity. Nat Aging, 2023. **3**(12): p. 1544-1560. https://doi.org/10.1038/s43587-023-00521-y
90. Nagai, M., R. Noguchi, D. Takahashi, et al., Fasting-refeeding impacts immune cell dynamics and mucosal immune responses. Cell, 2019. **178**(5): p. 1072-1087.e14. https://doi.org/10.1016/j.cell.2019.07.047
91. Schofield, J.H. and Z.T. Schafer, Mitochondrial reactive oxygen species and mitophagy: A complex and nuanced relationship. Antioxid Redox Signal, 2021. **34**(7): p. 517-530. https://doi.org/https://doi.org/10.1089/ars.2020.8058
92. Suzuki, K., K. Nakamura, Y. Shimizu, et al., Decrease of α-defensin impairs intestinal metabolite homeostasis via dysbiosis in mouse chronic social defeat stress model. Sci Rep, 2021. **11**(1): p. 9915. https://doi.org/10.1038/s41598-021-89308-y
93. Hu, T., C.H. Liu, M. Lei, et al., Metabolic regulation of the immune system in health and diseases: mechanisms and interventions. Signal Transduct Target Ther, 2024. **9**(1): p. 268. https://doi.org/10.1038/s41392-024-01954-6
94. Ivashkiv, L.B., IFNγ: signalling, epigenetics and roles in immunity, metabolism, disease and cancer immunotherapy. Nat Rev Immunol, 2018. **18**(9): p. 545-558. https://doi.org/10.1038/s41577-018-0029-z